

Department of Mechanical and Aerospace Engineering

Master degree course in Aerospace Engineering

Master Degree Thesis

Escape maneuvers using double lunar gravity assist



**POLITECNICO
DI TORINO**

Supervisor:

Lorenzo Casalino

Candidate:

Marco Campagnoli

March 2019

Acknowledgments

I would like to acknowledge my thesis advisor Professor Lorenzo Casalino of the Mechanics and Aerospace department at Politecnico of Turin. His help was essential for the realization of this work.

Thanks my friends and colleagues, Mauro Mancini, Francesco Biondi, Andrea Lin and Pasquale Megliola who have made these years of studies more pleasurable and helped me to overcome difficulties faced during the draft of this document.

Finally, I am grateful to my family, who always have supported me, although the distance. This achievement would not have been possible without them.

Thank you.

Contents

List of figure	v
List of tables	vii
1 Introduction	1
2 The two body problem	3
2.1 Equation of motion in an inertial frame	3
2.2 Constants of the motion	5
2.2.1 The angular momentum	6
2.2.2 Specific mechanical energy	7
2.2.3 Equation of the trajectory	8
2.2.4 Types of trajectories and orbits	10
3 Escape maneuvers	13
3.1 Method of patched conics	13
3.2 Hohmann transfer	14
3.3 Planetary departure	17
3.4 Gravity assist maneuvers	19
3.5 Coordinate systems	26
3.5.1 ECI system	26
3.5.2 Heliocentric system	27
3.5.3 Spherical coordinates	27

4	Analysis	29
4.1	Shooting method	29
4.2	Equation of motion	34
4.3	Perturbations	35
4.3.1	Earth asphericity	36
4.3.2	LuniSolar perturbation	36
4.3.3	Solar radiation pressure	38
4.4	Mass evaluation	39
5	Features of the mission	41
5.1	interplanetary leg: the ARM mission	41
5.2	Solar perturbed Moon to Moon leg	43
6	Results	47
6.1	Stepped procedure	49
6.2	Cases with different data and escape velocity	52
7	Conclusions	61
	Bibliography	63

List of figure

2.1	Free-body diagram of two masses in an inertial frame [1]	4
2.2	Plane of the orbit of the mass m_2 around m_1 identified by the vector \bar{h} [1]	7
2.3	Different types of path of the mass m_2 around a main body of mass m_1 .	11
3.1	Hohmann transfer from an inner planet 1 to an outer planet 2 [1]	15
3.2	Departure for an interplanetary mission from an inner planet to an outer planet [1]	18
3.3	Voyager 1 and Voyager 2 trajectories [13]	20
3.4	Artistic representation of the spacecraft Voyager 2 [14]	21
3.5	Cassini interplanetary trajectory [1]	21
3.6	Geometrical schema for a generic lunar gravity assist manoeuvre [9] . .	23
3.7	Components of \bar{V}_∞ expressed via pump (p) and crank (k) angles [9] . .	24
3.8	Leading-side flyby [1]	25
3.9	Trailing-side flyby [1]	25
3.10	J 2000 ECI reference system [16]	27
3.11	J 2000 heliocentric ecliptic reference system [16]	28
3.12	spherical coordinates	28
4.1	example of $p^{(r)}$ vector	33
4.2	Schematic geometry of gravitational perturbations [8]	37
5.1	Orbit of 2008 EV_5 (in white), position on 1st January 2010 [18]	42
5.2	different views of the 2008 EV_5 [18]	43

5.3	Families of solar-perturbed Moon-to-Moon transfers for an initial lunar relative velocity of 1 km/s. The Moons initial and final positions at the flybys are identified by black and green dots, respectively. Each family includes various trajectory that correspond to a different solar phase angle. To visually emphasize the differences between family members, all trajectories are rotated so that can start at the same lunar position [6]	44
5.4	Maximum escape C_3 vs declination when lunar-assisted escape is used [6]	45
6.1	in plane and out of plane views of the reference solution in the ecliptic inertial reference frame [6]	48
6.2	in plane and out of plane views of the reference solution in the Sun-Earth rotating frame [6]	48
6.3	First flyby of the Moon, the red line identifies the spacecraft trajectory, the blue line identifies Moon's path	49
6.4	effect of the solar perturbation on the orbit	50
6.5	effect of the solar perturbation on the orbit	50
6.6	case A, escape on the 18th of June, XY view	51
6.7	case A, escape on the 18th of June, YZ view	52
6.8	case B, escape on the 17th of June 2022, XY view	53
6.9	case B, escape on the 17th of June 2022, YZ view	53
6.10	case C, escape on the 19th of June 2022, XY view	54
6.11	case C, escape on the 19th of June 2022, YZ view	55
6.12	case C, a detailed view of the first flyby	55
6.13	case D, escape on the 20th of June 2022, XY view	56
6.14	case D, escape on the 20th of June 2022, YZ view	56
6.15	a comprehensive, in plane, view of the four different cases	57
6.16	a comprehensive, out of plane, view of the four different cases	57

List of tables

2.1	features of the different kind of trajectories and orbits	10
6.1	position in spherical coordinates for each phase of the different analyzed cases	58
6.2	times of the different analyzed cases	58
6.3	comparison of the velocities at the perigee and at the escape for the analyzed cases	59
6.4	energy comparison among the different solutions	60

Introduction

The space, as it is called everything placed beyond Earth's atmosphere, has always fascinated the human mind.

Astronomy, the observation of objects in space, is an ancient science that precedes reliable recorded history. It is only in the latter half of the 20th century, when were developed rockets powerful enough to overcome the force of gravity and to reach orbital velocities, that the physical space exploration become a practical possibility.

The early era of space exploration was driven by a "Space Race" between Unites States and Soviet Union. Two significant events mark the boundaries for this period: on October 4, 1957, occurs the launch of the first man-made object to orbit the Earth, the USSR's Sputnik 1, while on July 20, 1969, took place the first Moon landing by the American Apollo 11 spacecraft.

At present days, common rationales for exploring space include advancing scientific research, uniting different nations and ensuring the future survival of humanity. The International Space Station (ISS), which is a research laboratory in low Earth orbit, represents an important example of cooperation among different states all over the world.

Interplanetary missions is needed to study the planets, asteroids, and comets by their close proximity. An interplanetary mission is a voyage through the outer space that involves at least two different celestial bodies. A large number of robotic interplanetary missions have been performed by the NASA, the Soviet Union (and later by Roscosmos), Indian Space Research Organisation, Japan Aerospace Exploration Agency and the European Space Agency. However, until now, all manned missions have been in Earth's orbit or to the Moon. First, properly named, manned interplanetary mission will be, in all likelihood, one of the proposed human missions to Mars for the 2030s.

In many cases is not possible to deliver the required payload mass due to propulsion capabilities. In fact, the mass of propellant requested to developing the velocity change to accomplish the mission can represents the vast majority of the spacecraft mass (for example the 99 %, for an Earth-Saturn Hohmann transfer) if current chemical engine technology is used. For this reason a technique that produces a change in velocity

without having to resort to the propellant consumption becomes necessary. Gravity assist maneuvers are able to fulfill this task.

Gravity assists have been exploited in the past 50 years to reach targets with very high or very low energy orbits with respect to the Earth and also to considerably change the heliocentric orbit inclination. All these types of orbits are known under the category of high ΔV targets, due to the high ΔV budget necessary to reach them from Earth. The concept of gravity assist is illustrated in "Escape maneuvers".

The aim of this thesis is to evaluate an evasion maneuver with a double lunar gravity assist (LGA) for a future interplanetary mission (one possibility was the ARM mission described in "Features of the mission").

The analysis starts from an attempt of replicate a solution obtained in the paper "Design of Lunar-Gravity-Assisted Escape Maneuvres" [6], which is characterized by a phase between the two lunar encounters affected by the solar gravity attraction. This fact is caused by the high distance from Earth reached in this phase.

In order to obtain an exact numerical solution of the escape maneuver, the method must include solar gravity attraction and solar radiation pressure in addition to Earth asphericity and lunar perturbation. Each one of these terms is defined in "Analysis".

In the present document four different solutions are presented. They are characterized by different dates and, due to numerical convergence necessity, by different escape velocities. A comparison among these results is effectuated with the purpose of underlying the differences between them and to find the more efficient solution. This study is conducted in "Results".

The two body problem

The two body problem describes the interaction between two masses caused by their own mutual gravity attraction. The motion of a body around another one can be defined by using this approach. The trajectory of the mass is a conic section (circle, ellipse, parabola or hyperbola) depending on the value of the eccentricity. Typically, the main body has an higher mass compared to the secondary body. They are modelled as point masses located in the mass center of the relative bodies.

This problem descent from the N-body problem, which is the complete case of study, talking about the motion of a celestial body. For example the Earth's revolution is influenced, in addition to the Sun's gravity field, by the gravity attraction of: Moon, Mars, Venus, Mercury, Juno, Saturn and also by Ceres (the largest asteroid of the asteroid belt, classified as a dwarf planet). Considering the higher distance, Uranus, Neptune and Pluto have a smaller effects on the Earth's orbit.

If all the effects of these bodies are taking into account, a numerical integration is needed to identify a solution. The two body problem allows to obtain an analytic solution by limiting the problem solely to a main and a secondary body.

2.1 Equation of motion in an inertial frame

Figure 2.1 shows the position of the two bodies, which are represented as point masses relative to the inertial reference frame XYZ. The origin of the frame "O" may have a constant velocity (relative to the fixed stars), but the axes can't rotate. Each of the two masses is subjected to the gravitational attraction of the other. The force that the mass m_2 exerting on m_1 is identified by the vector \overline{F}_{12} . According to Newton's third law (the action-reaction principle) the mass m_2 applies the force \overline{F}_{21} over the the mass m_1 .

The position vector of m_2 relative to m_1 is identified by the vector \overline{r} , which is:

$$\overline{r} = \overline{R}_2 - \overline{R}_1 \tag{2.1}$$

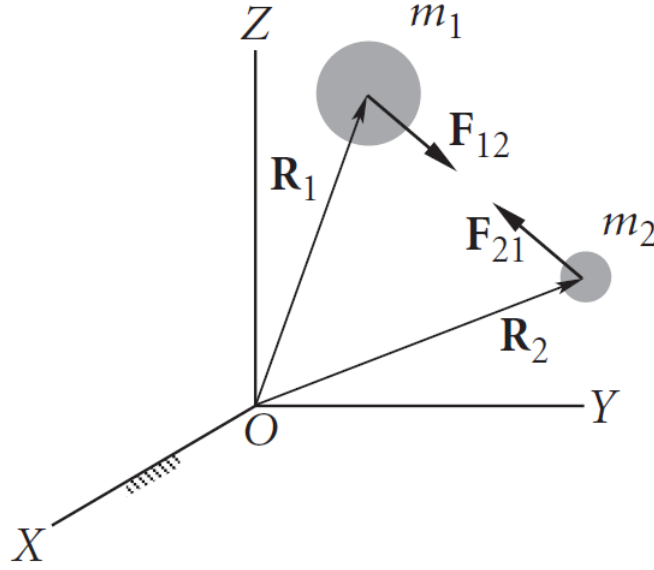


Figure 2.1: Free-body diagram of two masses in an inertial frame [1]

Assume \hat{u}_r as the unit vector that points from m_1 to m_2 , so:

$$\hat{u}_r = \frac{\bar{r}}{r} \quad (2.2)$$

where $r = \|\bar{r}\|$ is the magnitude of \bar{r} .

Newton's law of universal gravitation is used:

$$\bar{F}_{21} = -\frac{Gm_1m_2}{r^2}\hat{u}_r \quad (2.3)$$

in which the minus sign takes into account the fact that the force vector \bar{F}_{21} points from m_2 towards m_1 .

It is important to note that the gravitational force is inversely proportional to the square of the distance between the two masses and it is directed along their joining line.

G is the gravitational constant, which values $6.674 * 10^{-11} \frac{m^3}{Kg*s^2}$.

Newton's third law imposes $\bar{F}_{12} = -\bar{F}_{21}$, meaning that for m_1 is possible to write:

$$\frac{Gm_1m_2}{r^2}\hat{u}_r = m_1\ddot{\bar{R}}_1 \quad (2.4)$$

where also Newton's second law of motion is applied. In the same way, $m_2 : \bar{F}_{12} = m_2\ddot{\bar{R}}_2$, with $\ddot{\bar{R}}_2$ as the absolute acceleration of m_2 . Therefore:

$$-\frac{Gm_1m_2}{r^2}\hat{u}_r = m_2\ddot{R}_2 \quad (2.5)$$

Equations 2.5 and 2.4 are the equations of motion of the two bodies in an inertial space. At this point, equation 2.5 is multiplied by m_1 and equation 2.4 by m_2 , thus:

$$-\frac{Gm_1^2m_2}{r^2}\hat{u}_r = m_1m_2\ddot{R}_2 \quad (2.6)$$

$$\frac{Gm_1m_2^2}{r^2}\hat{u}_r = m_1m_2\ddot{R}_1 \quad (2.7)$$

By subtracting equation 2.7 to 2.6 we obtain:

$$m_1m_2(\ddot{R}_2 - \ddot{R}_1) = -\frac{Gm_1m_2}{r^2}(m_1 + m_2)\hat{u}_r \quad (2.8)$$

The terms m_1 and m_2 can be eliminated and equation 2.1 used:

$$\ddot{\vec{r}} = -\frac{G(m_1 + m_2)}{r^2}\hat{u}_r \quad (2.9)$$

The gravitational parameter μ is identified as:

$$\mu = G(m_1 + m_2) \quad (2.10)$$

μ is expressed in km^3/s^2 . Equations 2.9 and 2.10 can be combined together to obtain:

$$\ddot{\vec{r}} = -\frac{\mu}{r^3}\vec{r} \quad (2.11)$$

Equation 2.11 is a second order differential equation. This equation governs the motion of m_2 with respect to m_1 . It is composed by three scalar components, so it is characterized by six constants of integration in two vector constants made up of three scalar components.

Equation 2.11 can be multiplied through by -1 in order to note that is possible to exchange the roles of m_1 and m_2 in the above amounts. Therefore, the motion of m_2 as seen from m_1 is exactly the same as the motion of m_1 as seen from m_2 .

2.2 Constants of the motion

Two significant quantities must be introduced before the integration of the equations of motion, they are: the specific angular momentum h and the specific mechanical energy \mathcal{E} .

2.2.1 The angular momentum

The body m_2 has an angular momentum relative to m_1 , which can be defined as:

$$\overline{H}_{21} = \overline{r} \times m_2 \dot{\overline{r}} \quad (2.12)$$

dividing this equation by m_2 leads to:

$$\overline{h} = \frac{\overline{H}_{21}}{m_2} = \overline{r} \times \dot{\overline{r}} \quad (2.13)$$

where $\dot{\overline{r}} = \overline{V}$ is the velocity of m_2 with respect to m_1 .

The specific relative angular momentum, h , is the relative angular momentum of m_2 per unit mass. It is expressed in km^2/s .

Starting from equation 2.11 first and second terms of the equation are left cross multiplied by \overline{r} , so that:

$$\overline{r} \times \ddot{\overline{r}} = -\overline{r} \times \frac{\mu}{r^3} \overline{r} \quad (2.14)$$

Considering that a vector is always parallel to itself, so that: $r \times r = 0$, the second term of the equation 2.14 is going to zero. Therefore:

$$\overline{r} \times \ddot{\overline{r}} = 0 \quad (2.15)$$

Taking into account that:

$$\frac{d}{dt}(\overline{r} \times \dot{\overline{r}}) = \overline{r} \times \ddot{\overline{r}} + \dot{\overline{r}} \times \dot{\overline{r}} \quad (2.16)$$

also in this case, is possible to point out that: $\dot{\overline{r}} \times \dot{\overline{r}} = 0$, due to the reason illustrated before.

Finally, since that the term $(\overline{r} \times \dot{\overline{r}})$ has a null derivative, is possible to identify the specific angular momentum: $h = \overline{r} \times \overline{V}$ as a constant of the motion.

The definition of cross products establish the perpendicularity between \overline{r} and \overline{V} , by its very nature. The fact that the angular momentum is constant in magnitude and direction means that \overline{r} and \overline{V} will always lie on the same plane. Therefore, Newtonian orbits are characterized by a fixed plane of motion, which is called orbital plane.

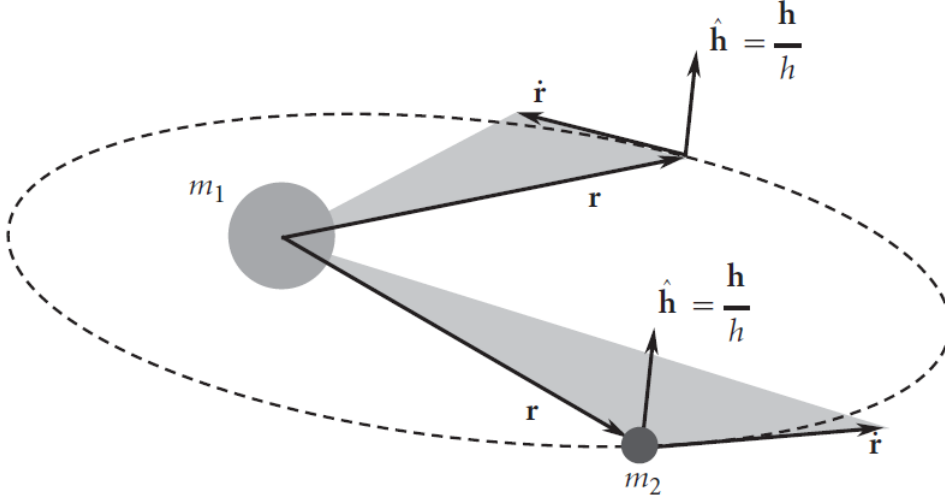


Figure 2.2: Plane of the orbit of the mass m_2 around m_1 identified by the vector \bar{h} [1]

2.2.2 Specific mechanical energy

The specific mechanical energy \mathcal{E} is defined as the sum of kinetic and potential energy per unit mass. Its units are km^2/s^2 .

Starting from equation 2.11, both members are multiplied by \bar{r} , so that:

$$\dot{\bar{r}} \cdot \ddot{\bar{r}} + \dot{\bar{r}} \cdot \frac{\mu}{r^3} \bar{r} = 0 \quad (2.17)$$

That is equivalent to:

$$\dot{r} \ddot{r} + \dot{r} \frac{\mu}{r^2} = 0 \quad (2.18)$$

Remembering that $\dot{\bar{r}} = V$, is possible to write:

$$\begin{cases} V\dot{V} = \frac{d}{dt} \left(\frac{V^2}{2} \right) \\ \dot{r} \frac{\mu}{r^2} = \frac{d}{dt} \left(-\frac{\mu}{r} \right) \end{cases} \quad (2.19)$$

So that:

$$\frac{d}{dt} \left(\frac{V^2}{2} - \frac{\mu}{r} \right) = 0 \quad (2.20)$$

Finally, the energy equation can be written:

$$\mathcal{E} = \frac{V^2}{2} - \frac{\mu}{r} + C = \text{const.} \quad (2.21)$$

which taking into account:

- $\frac{V^2}{2}$, that represents the specific kinetic energy and expresses the energy contribution caused by the motion;
- $-\frac{\mu}{r}$, which is the specific potential energy, it represents the contribution given by the gravity field, that depends only on the mass of the main body and on the position on the secondary body;
- C , which is a constant term that is given by the integration of equation 2.20 and has an arbitrary value. Choosing the zero reference for potential energy at infinity allows to set this constant equal to zero.

2.2.3 Equation of the trajectory

Now that constant of the motion have been defined, is possible to integrate twice equation 2.11 in order to obtain the trajectory equation of the two body problem. Nevertheless, before the integration is convenient to manipulate the starting equation to highlight the derivative.

Firstly, it is left cross multiplied by the specific angular momentum vector \bar{h} :

$$\ddot{\bar{r}} \times \bar{h} = -\frac{\mu}{r^3} \bar{r} \times \bar{h} \quad (2.22)$$

That can be rewritten as:

$$\ddot{\bar{r}} \times \bar{h} = \frac{\mu}{r^3} (\bar{h} \times \bar{r}) \quad (2.23)$$

In the first member of the equation 2.23 a derivative can be easily identified as:

$$\frac{d}{dt} (\dot{\bar{r}} \times \bar{h}) = (\ddot{\bar{r}} \times \bar{h}) + (\dot{\bar{r}} \times \dot{\bar{h}}) \quad (2.24)$$

where the second term in the right side can be canceled, knowing that \bar{h} is a constant of the motion. Thus:

$$\frac{d}{dt}(\dot{\bar{r}} \times \bar{h}) = (\ddot{\bar{r}} \times \bar{h}) \quad (2.25)$$

On the other hand, for the second member is possible to write:

$$\frac{\mu}{r^3}(\bar{h} \times \bar{r}) = \frac{\mu}{r^3}(\bar{r} \times \bar{V}) \times \bar{r} = \quad (2.26)$$

$$= \frac{\mu}{r^3}[\bar{V}(\bar{r} \cdot \bar{r}) - \bar{r}(\bar{r} \cdot \bar{V})] = \quad (2.27)$$

$$= \frac{\mu}{r}\bar{V} - \frac{\mu\dot{\bar{r}}}{r^2}\bar{r} = \quad (2.28)$$

$$= \mu \frac{d}{dt}\left(\frac{\bar{r}}{r}\right) \quad (2.29)$$

Therefore, equation 2.11 can be rewritten as:

$$\frac{d}{dt}(\dot{\bar{r}} \times \bar{h}) = \mu \frac{d}{dt}\left(\frac{\bar{r}}{r}\right) \quad (2.30)$$

that is integrated and lead to:

$$\dot{\bar{r}} \times \bar{h} = \mu \frac{\bar{r}}{r} + \bar{B} \quad (2.31)$$

in which \bar{B} is the constant vector that comes from the integration.

At this point, equation 2.31 is dot multiplied by \bar{r} :

$$\bar{r} \cdot \dot{\bar{r}} \times \bar{h} = \mu \frac{\bar{r} \cdot \bar{r}}{r} + \bar{r} \cdot \bar{B} \quad (2.32)$$

By developing the scalar product:

$$h^2 = \mu r + rB \cos(\nu) \quad (2.33)$$

that is the desired equation, which can be solved for r in order to obtain the following trajectory equation:

$$r = \frac{h^2/\mu}{1 + \frac{B}{\mu} \cos(\nu)} \quad (2.34)$$

equation 2.34 represent, in polar coordinates, the equation of a conic section with its origin in one of the foci.

Finally, if equation 2.34 is rewritten as:

$$r = \frac{p}{1 + e \cos(\nu)} \quad (2.35)$$

is possible to identify: the semilatus rectum p , the eccentricity e and the angle ν , that is the angle between periapsis (the point of the orbit which is closest to the focus of the conic section) and \bar{r} .

2.2.4 Types of trajectories and orbits

The words trajectory and orbit both refer to the path of a body in space. Trajectory is commonly associated with paths of limited extent, i. e., paths having clearly identified initial and end points. Orbit is commonly used with paths that are more or less indefinitely extended or of a repetitive character, like the orbit of the Moon around the Earth. In discussions of space flight, both terms are used, with the choice usually dependent upon the nature of the flight path. Therefore, we talk about trajectories from the Earth to Moon, and of planets orbits around the Sun.

In table 2.1 and in figure 2.3 are illustrated the characteristics of the different types of trajectories and orbits.

trajectory type	eccentricity	major semi-axis	energy	V_∞
circular	$e = 0$	$a > 0$	$\mathcal{E} < 0$	—
elliptical	$0 < e < 1$	$a > 0$	$\mathcal{E} < 0$	—
parabolic	$e = 1$	$a \rightarrow \infty$	$\mathcal{E} = 0$	$V_\infty = 0$
hyperbolic	$e > 1$	$a < 0$	$\mathcal{E} > 0$	$V_\infty > 0$

Table 2.1: features of the different kind of trajectories and orbits

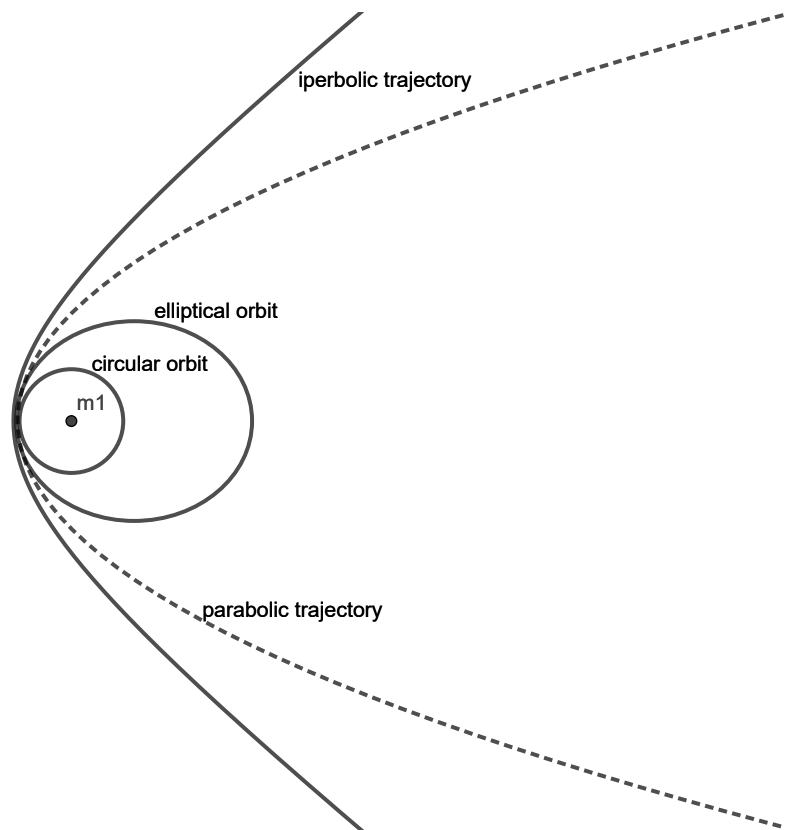


Figure 2.3: Different types of path of the mass m_2 around a main body of mass m_1

Escape maneuvers

In order to be on the way to the destination celestial body, target of the space mission, it is necessary, first of all, to climb out of the potential well of the originating planet.

A spacecraft that travels on a parabolic trajectory, relative to the planet, will arrive at the sphere of influence with a relative speed of zero. With a view to obtain a propellant save, is possible to perform an hyperbolic trajectory, arriving at the sphere's boundary with a relative velocity V_∞ (hyperbolic excess velocity) greater than zero. In that case the spacecraft embarks upon a heliocentric elliptical path, leaving the orbit of the planet.

Therefore, an interplanetary mission can be divided into three parts:

- the hyperbolic trajectory relative to the departure planet;
- the interplanetary trajectory, relative to the sun;
- the hyperbolic arrival trajectory, relative to the target celestial body.

3.1 Method of patched conics

The noun 'conics' descends from the fact that two-body or Keplerian orbits are conic sections having a focus coincident with the attracting body. Is possible to study an interplanetary trajectory under the assumption that the spacecraft follows an unperturbed Keplerian orbit around the sun when it is outside the sphere of influence of the planet. On the other hand, the spacecraft describes another unperturbed Keplerian path around the planet within each planetary sphere of influence.

While the sphere of influence appears as a mere speck on the scale of the solar system, from the point of view of the planet it is very large indeed and may be considered to lie at infinity.

The sphere of influence (SOI) is a concept that generally involves: a planet of mass m_p , the Sun of mass m_s and a spacecraft of mass $m_{s/c}$ (negligible mass). Essentially, this is

the region in which the gravitational attraction of the planet overwhelms the attraction of the sun.

One way to determine the radius of the sphere of influence is to calculate the distance between the planet's center of gravity and the points at which the perturbing effect of the sun on the vehicle's orbit around the planet is equal to the perturbing effect of the planet on the vehicle's orbit around the sun.

This approach leads to the equation of the Lagrangian sphere of influence:

$$\frac{r_{SOI}}{R} = \left(\frac{m_p}{m_s} \right)^{\frac{2}{5}} \quad (3.1)$$

where R is the distance between the planet and the Sun and r_{SOI} is the radius of the sphere of influence.

For example, for our planet, giving:

$$\begin{cases} m_{earth} = 5.974 * 10^{24} \text{ Kg} \\ m_{sun} = 1.989 * 10^{30} \text{ Kg} \\ R_{earth} = 149.6 * 10^6 \text{ Km} \end{cases}$$

is possible to determine:

$$r_{SOI} = 149.6 * 10^6 * \left(\frac{5.974 * 10^{24}}{1.989 * 10^{30}} \right)^{\frac{2}{5}} = 0.925 * 10^6 \text{ Km}$$

it means that the SOI of the Earth is about 1 million of Km, while the distance between the Earth and the Sun, which is used as a scale for our solar system and for the the interplanetary trajectories that are involved, is about 150 million of Km. Comparing this two quantities is clear how is it possible to use the patched conics approach that neglect the dimension of SOI and to consider them, like the planets they surround, to be just points in space coinciding with the planetary centers.

Finally, it is mandatory to remember that the Lagrangian sphere of influence is an approximated model useful only for a preliminary analysis of an interplanetary mission.

3.2 Hohmann transfer

The heliocentric phase usually consists of an Hohmann trajectory from planet 1 towards a target planet 2 which is, in this case, more distant from the sun (as in Figure 3.1).

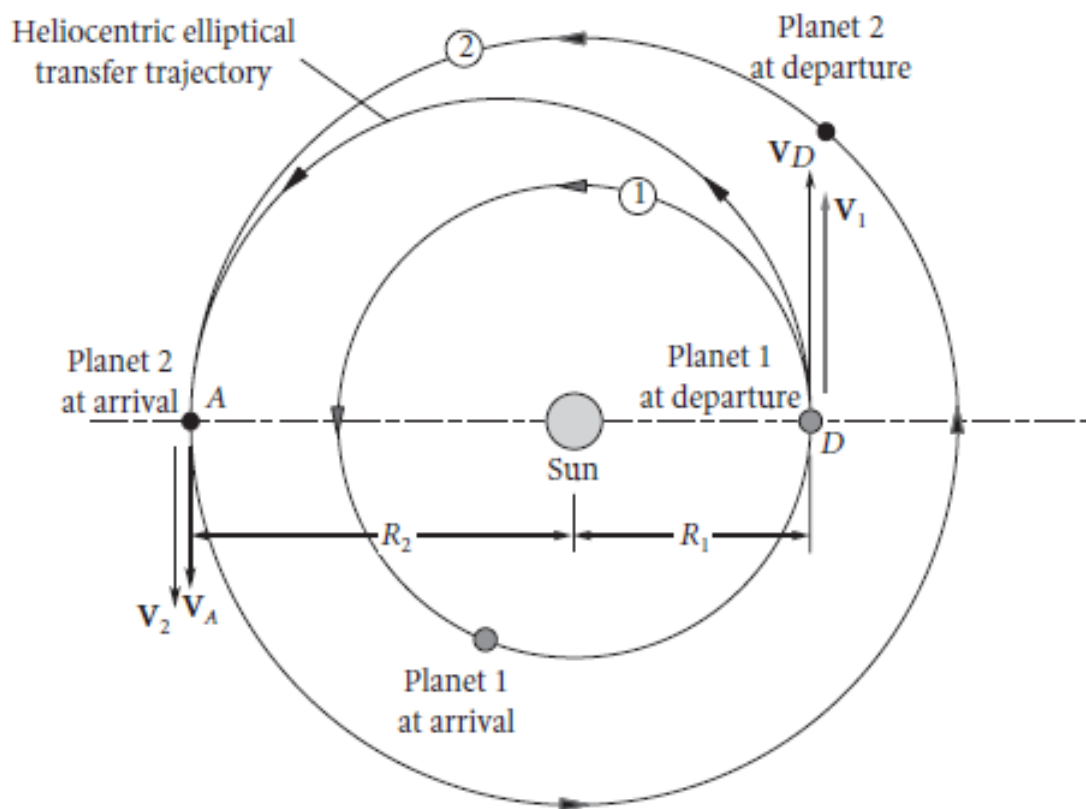


Figure 3.1: Hohmann transfer from an inner planet 1 to an outer planet 2 [1]

Hohmann transfer ellipse is the most energy efficient way for a spacecraft to transfer from an orbit around planet 1 to another around the target planet 2. The transfer ellipse starts from the departure point D, at the perihelion, and finishes on the arrival point A, at the aphelion.

The circular orbital speed of planet 1 relative to the sun is given by:

$$V_1 = \sqrt{\frac{\mu_s}{R_1}} \quad (3.2)$$

while the angular momentum in term of periapse ad apoapse radii is:

$$h = \sqrt{2\mu} \sqrt{\frac{r_a r_p}{r_a + r_p}} \quad (3.3)$$

is therefore possible to evaluate the velocity of the space vehicle on the transfer ellipse at the departure point D:

$$V_D = \frac{h}{R_1} = \sqrt{2\mu_s} \sqrt{\frac{R_2}{R_1(R_1 + R_2)}} \quad (3.4)$$

At the sphere of influence crossing, the heliocentric velocity V_D of the spacecraft is parallel to the asymptote of the departure hyperbola as well as to the planet's heliocentric velocity vector V_1 . This leads to the fact that only the magnitude can be added up, not the vectors. V_D and V_1 must be parallel and in the same direction for a Hohmann transfer such that ΔV_D is positive. Clearly, the hyperbolic excess speed of the departure hyperbola V_∞ , is identical to ΔV_D and can be determined by the following equation:

$$\Delta V_D = V_D - V_1 = \sqrt{\frac{\mu_s}{R_1}} \left(\sqrt{\frac{2R_2}{R_1 + R_2}} - 1 \right) \quad (3.5)$$

in the same way the ΔV at the arrival point A is:

$$\Delta V_A = V_2 - V_A = \sqrt{\frac{\mu_s}{R_2}} \left(1 - \sqrt{\frac{2R_1}{R_1 + R_2}} \right) \quad (3.6)$$

As we can see in figure 3.1, the velocity change at point A and D is grater than zero, since we transfer to orbits with augmented semi-major axis, that are characterized by an higher energy.

The same two ΔV will be both negative if the mission is directed to an inner planet, because of departure point and arrival point are now at aphelion and perihelion, respectively, of the transfer ellipse. At the departure point D the speed of the spacecraft must be reduced

because it drop into the lower-energy transfer ellipse (with a reduced semi-major axis) and it must be reduced again at point A in order to arrive in the lower-energy circular orbit of planet 2.

3.3 Planetary departure

The required conditions at the escape, necessary to reach a celestial body target, are been evaluated, now is possible to discuss about the geocentric phase that realize these conditions.

The spacecraft starts its interplanetary trajectory from a circular parking orbit, whose radius equals the perigee radius r_p of the departure hyperbola. Using the energy equation, it is easily to determine the semi-major axis, a , as also the ΔV required to achieve the desired trajectory, knowing the value of the hyperbolic excess velocity V_∞ (which is the ΔV_D calculated before) and of the perigee radius r_p .

$$\mathcal{E} = \frac{V_\infty^2}{2} = -\frac{\mu_E}{2a} \quad (3.7)$$

thus:

$$a = -\frac{\mu_E}{V_\infty^2} \quad (3.8)$$

Also, equation 3.7 can be rewritten as:

$$\mathcal{E} = \frac{V_P^2}{2} - \frac{\mu_E}{r_p} = \frac{V_\infty^2}{2} \quad (3.9)$$

and so:

$$V_P = \sqrt{V_\infty^2 + \frac{2\mu_E}{r_p}} \quad (3.10)$$

with the velocity of the circular parking orbit defined by:

$$V_{P0} = \sqrt{\frac{\mu_E}{r_p}}$$

The required ΔV to leave the parking orbit is: $\Delta V = V_P - V_{P0}$

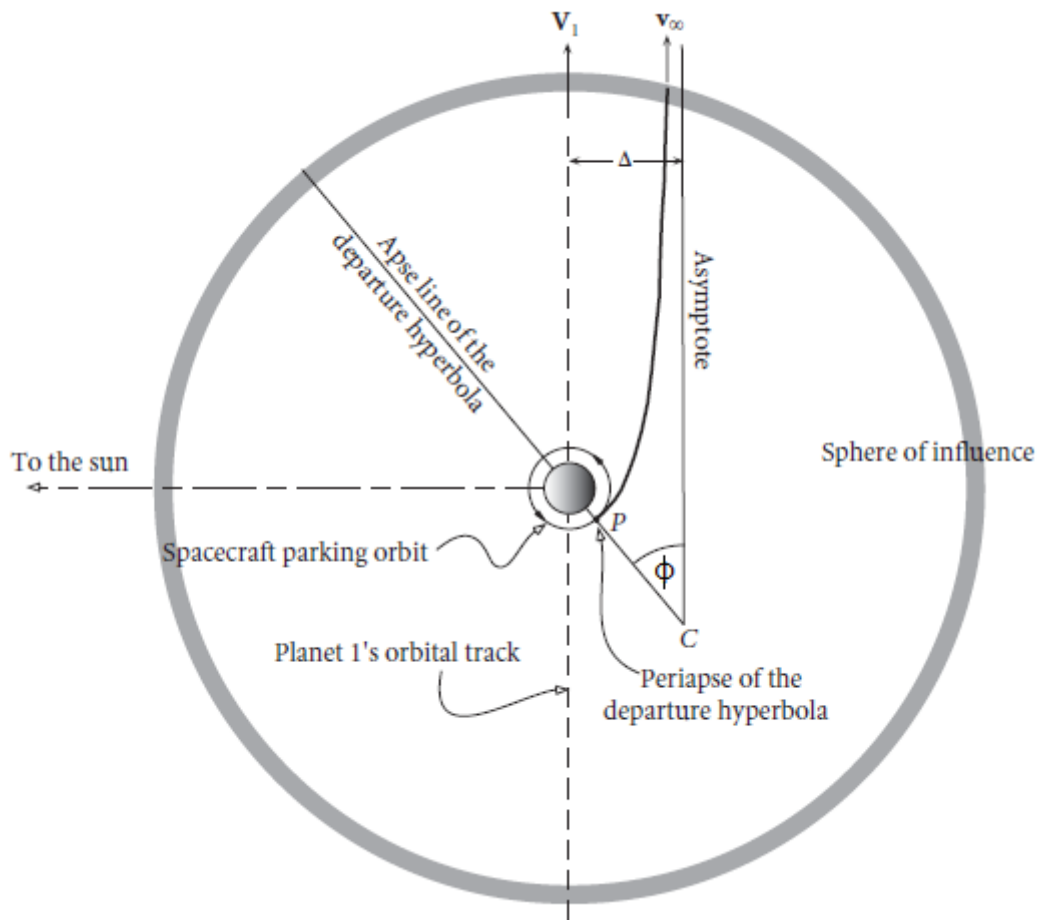


Figure 3.2: Departure for an interplanetary mission from an inner planet to an outer planet [1]

The angle Φ , in figure 3.2, identifies the orientation of the apses line of the hyperbola to the hyperbolic excess velocity V_∞ , which is parallel to the planet's heliocentric velocity vector V_1 , as said above. It can be calculated as:

$$\Phi = \arccos\left(\frac{1}{e}\right) \quad (3.11)$$

Therefore, the eccentricity of hyperbola is needed. The equation of semilatus rectum can be written:

$$p = \frac{h^2}{\mu_E} = a(1 - e^2) = r_p(1 + e) \quad (3.12)$$

in which is used h , the angular momentum of the departure hyperbola, that is (relative to the departure planet):

$$h = r_p V_p$$

So the eccentricity of the escape trajectory can be evaluated as:

$$e = \frac{r_p V_p^2}{\mu_E} - 1 \quad (3.13)$$

At this point, is possible to go back to equation 3.11 and to calculate the value of the angle Φ .

The case depicted refers to a *front door exit* and can be seen in figure 3.2.

On the other side, if the mission consists to sent a spacecraft from an outer planet to an inner planet, the space vehicle must emerge from the backside of the sphere of influence with a relative velocity opposite directed respect to V_1 , that cause a reduction of the heliocentric velocity. This is a case of *back door exit*.

3.4 Gravity assist maneuvers

Since they can significantly change the heliocentric velocity of a spacecraft without using propellant, gravity assist maneuvers are a widely used technique to save fuel.

These maneuvers can be used to accelerate a spacecraft, that is, to increase or decrease its speed or to redirect its path. Angular momentum is transferred from the orbiting planet to a spacecraft approaching the planet in its progress about the sun.

The idea was first proposed by astronomical pioneers Yuri Kondratyuk and Friedrich Zander in their papers published in 1925 and 1938, respectively. It was first implemented

in 1959 by the Soviet probe Luna 3 to photograph the far side of the Moon. Since then, notable successful implementations include space probes: Mariner 10, Voyager 1 and 2, and Cassini.

On September 1977 Voyager 1 was launched and 2 years later, it performed a flyby of Jupiter (March 1979) used to reach Saturn in November 1980. Following, in August 1977 Voyager 2 started its ‘grand tour’ of the outer planets. Its journey involved gravity assist flybys of Jupiter (July 1979), Saturn (August 1981), Uranus (January 1986) and Neptune (August 1989), after which the spacecraft departed at an angle of 30° to the ecliptic. The two probes have now reached the interstellar space and represent the most distant human-made objects from Earth.

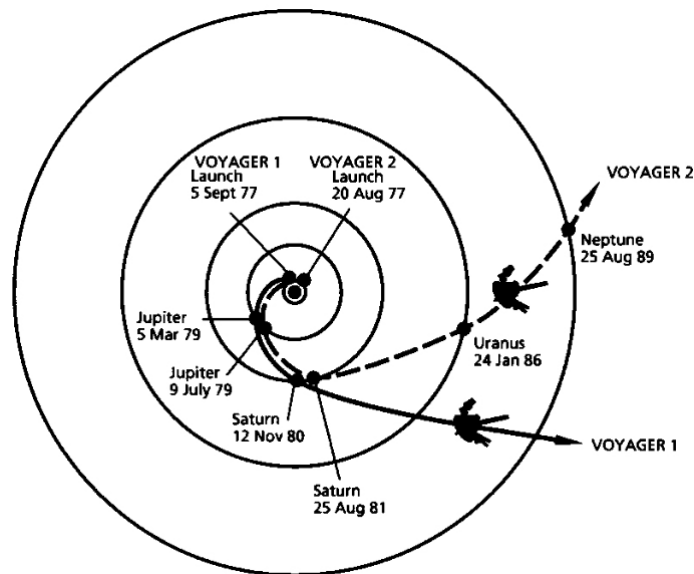


Figure 3.3: Voyager 1 and Voyager 2 trajectories [13]

The international Cassini mission to Saturn also made an extensive use of gravity assist flyby maneuvers. The Cassini spacecraft was launched on 15 October 1997 from Cape Canaveral, Florida, and arrived at Saturn nearly seven years later, on 1 July 2004. The mission involved four flybys. A little over eight months after launch, on 26 April 1998, Cassini flew by Venus at a periapse altitude of 284 km and received a speed boost of about 7 km/s. This placed the spacecraft in an orbit which sent it just outside the orbit of Mars (but well away from the planet) and returned it to Venus on 24 June 1999 for a second flyby, this time at an altitude of 600 km. The result was a trajectory that vectored Cassini toward the earth for an 18 August 1999 flyby at an altitude of 1171 km. The 5.5 km/s speed boost at earth sent the spacecraft toward Jupiter for its next flyby maneuver. This occurred on 30 December 2000 at a distance of 9.7 million km from Jupiter, boosting Cassini’s speed by about 2 km/s and adjusting its trajectory so as to rendezvous with Saturn about three and a half years later.

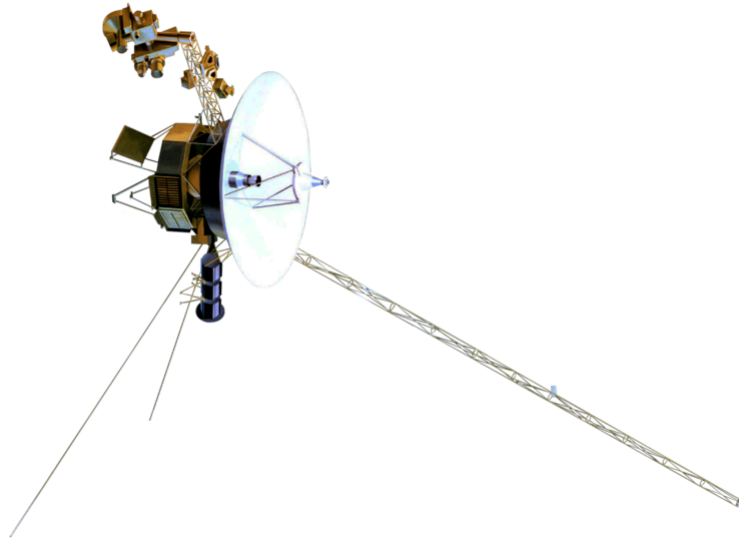


Figure 3.4: Artistic representation of the spacecraft Voyager 2 [14]

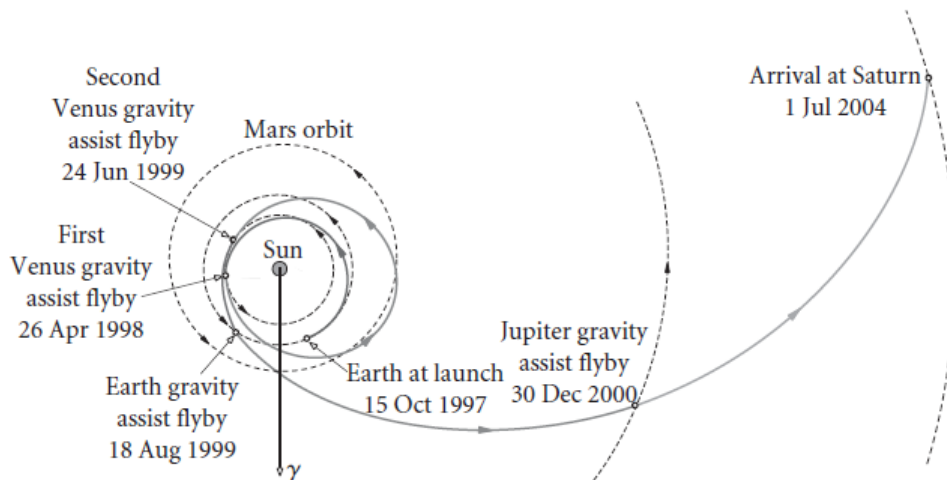


Figure 3.5: Cassini interplanetary trajectory [1]

A planetary flyby occurs when a spacecraft enters a planet's sphere of influence and does not landing on the planet or going into orbit around it. The s/c will continue in its hyperbolic trajectory through the periapsis and come back outside of the sphere of influence.

In particular, in this section the case of a spacecraft that realizes a lunar gravity assisted maneuver is illustrated.

The patched conics method is applied, so starting from the point where the spacecraft goes inside Moon's sphere of influence, the system can be described by the 2-body problem model, in which Earth's satellite represents the main body and the spacecraft represents the orbiting body. A planar maneuver is chosen for the sake of simplicity.

In Figure 3.6 a schematic representation of the problem is provided.

As the 2-body problem is used, at the edge of the lunar sphere of influence the velocity vector needs to be transformed from a geocentric reference velocity $\overline{V}_{S/C}$ to a velocity in the lunar reference frame, so the Moon's velocity \overline{V}_M is taking into account by using:

$$\overline{V}_{\infty}^{-} = \overline{V}_{S/C}^{-} - \overline{V}_M \quad (3.14)$$

Lunar orbital velocity \overline{V}_M and hyperbolic inbound velocity $\overline{V}_{\infty}^{-}$ are divided by the so called pump angle, that is, in detail for this case, the pump angle before LGA (p^{-}) and represents a significant quantity for evaluating the effectiveness of the maneuver.

At this point, considering that $\overline{V}_{\infty}^{-}$ has been evaluated and remembering that the spacecraft starts to orbit around the Moon since the moments that enters lunar sphere of influence (that can be approximated by $r \rightarrow \infty$, so a grater than zero V_{∞}^{-} is needed in order to pass through a periselenium higher than the moon radius and to avoid impact), the spacecraft is heading to escape the sphere of influence with a relative velocity $\overline{V}_{\infty}^{+}$.

Is possible to write the conservation of mechanical energy at the edge of the lunar sphere of influence, so that the equivalence $V_{\infty}^{-} = V_{\infty}^{+}$ has been demonstrated.

$$\mathcal{E} = \frac{(V_{\infty}^{-})^2}{2} - \frac{\mu}{r} = \frac{(V_{\infty}^{+})^2}{2} - \frac{\mu}{r} \quad (3.15)$$

where the gravitational terms $\frac{\mu}{r}$ tends to 0, taking into account that $r \rightarrow \infty$ at the edge of the SOI.

On the other hand, the angle $\delta = \pi - 2\phi$, in which $\phi = \arccos(1/e)$ stands as the opening angle of the hyperbola's eccentricity "e", describes the variation related to the direction of the vector \overline{V}_{∞} .

For the same reason, the angle between \overline{V}_{∞} and \overline{V}_M varying as well. Thus $p^{-} \neq p^{+}$ and consequently:

$$\bar{V}_{S/C}^+ = \bar{V}_M + \bar{V}_\infty^+ \neq \bar{V}_{S/C}^- \quad (3.16)$$

The usefulness of the gravity assist maneuver is then represented by a change of the heliocentric (or geocentric, when talking about LGA) velocity without using propellant. Conservation of angular momentum for the moon-spacecraft system can be used to explain the character of this ΔV :

$$\Delta H = m r_s \Delta V - M_M r_s \Delta V_M = 0 \quad (3.17)$$

where r_s is the radius of the Moon's sphere of influence.

Then, by simplifying r_s :

$$\Delta V_M = \frac{m}{M_M} \Delta V \quad (3.18)$$

A comparison between spacecraft's mass and lunar mass can be carried out, giving $m \ll M_M$ is possible to assume that the effect on the moon's velocity is negligible.

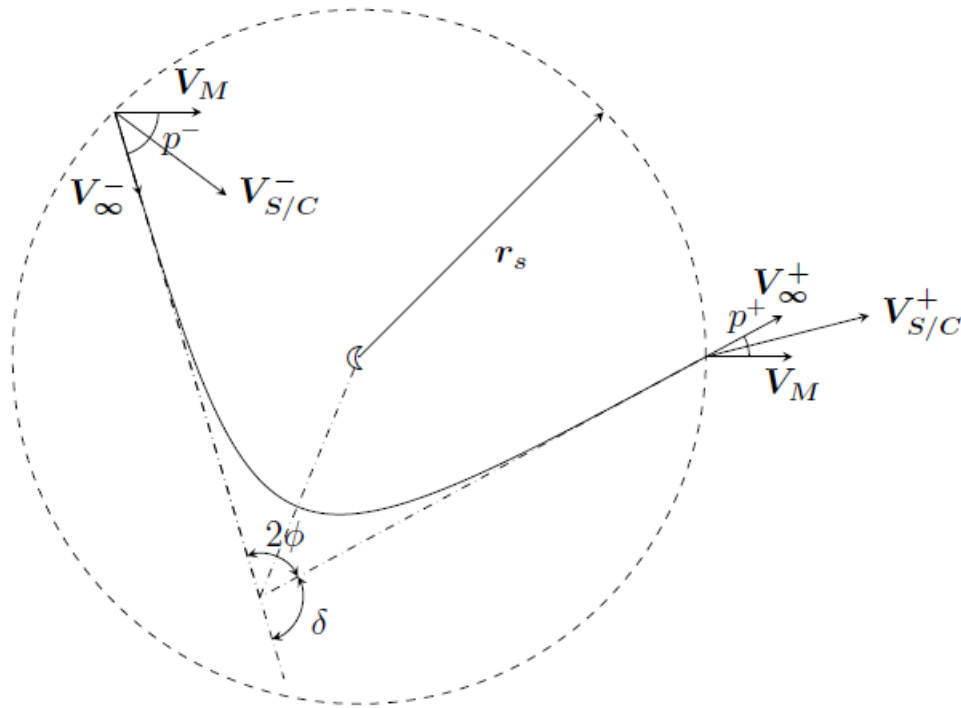


Figure 3.6: Geometrical schema for a generic lunar gravity assist manoeuvre [9]

As a complement, also the crank angle has to be defined in order to deal with a more general case, in which also a change in the orbital inclination takes place, meaning that

a Δi exists in addition to the ΔV . Finally the components of the velocity vector: radial, tangential, and normal are shown in figure 3.7.

$$\begin{cases} u_\infty = V_\infty \sin p \cos k \\ v_\infty = V_\infty \cos p \\ w_\infty = V_\infty \sin p \sin k \end{cases} \quad (3.19)$$

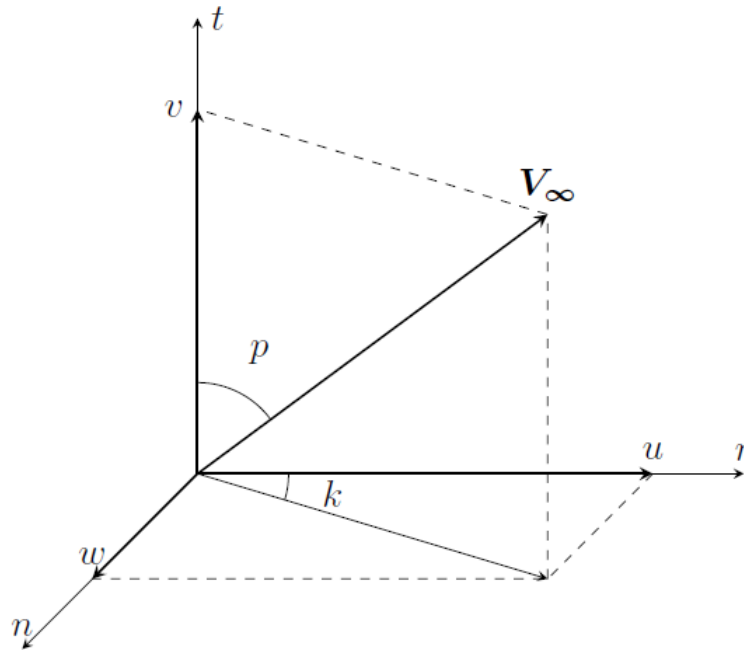


Figure 3.7: Components of \bar{V}_∞ expressed via pump (p) and crank (k) angles [9]

Finally, an important feature distinguishes two different kinds of flyby:

- leading-side flyby, which has the periapsis of the hyperbola on the side of the planet that faces the direction of motion of the encountered body.
- trailing-side flyby, which has the periapsis of the hyperbola on the side of the planet that is opposed to the direction of motion of the encountered body.

As long as the outbound hyperbolic velocity $V_{\infty 2}$ is directed in the opposite side of the planet orbital velocity V , a decrease of the heliocentric velocity is shown. In Figure 3.8 this result can be noted by observing that V_2 has a smaller module than V_1 for the case of a leading-side flyby. On the other hand, in Figure 3.9 is illustrated a case of trailing-side flyby, which produces an increase of the heliocentric velocity ($V_2 > V_1$). In this kind of flyby $V_{\infty 2}$ points to the same direction of the planet orbital velocity V .

An analogue discussion can be conducted in the case of a lunar flyby with the adjustment of using geocentric velocities in place of heliocentric velocities.

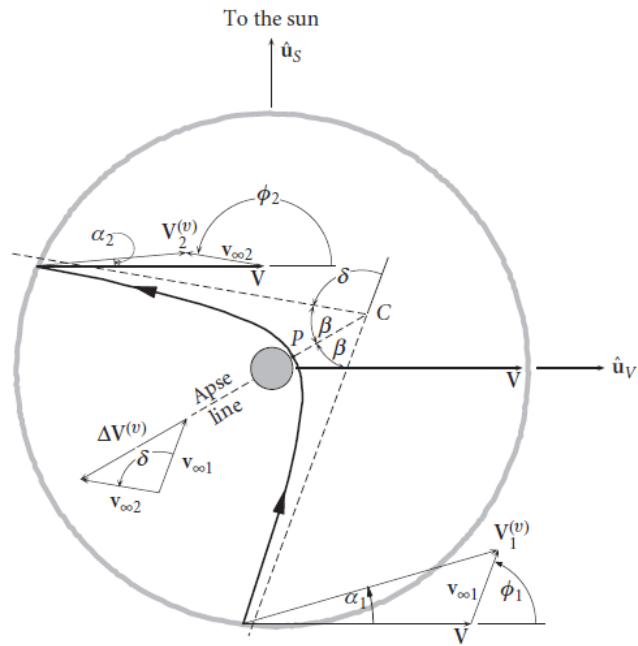


Figure 3.8: Leading-side flyby [1]

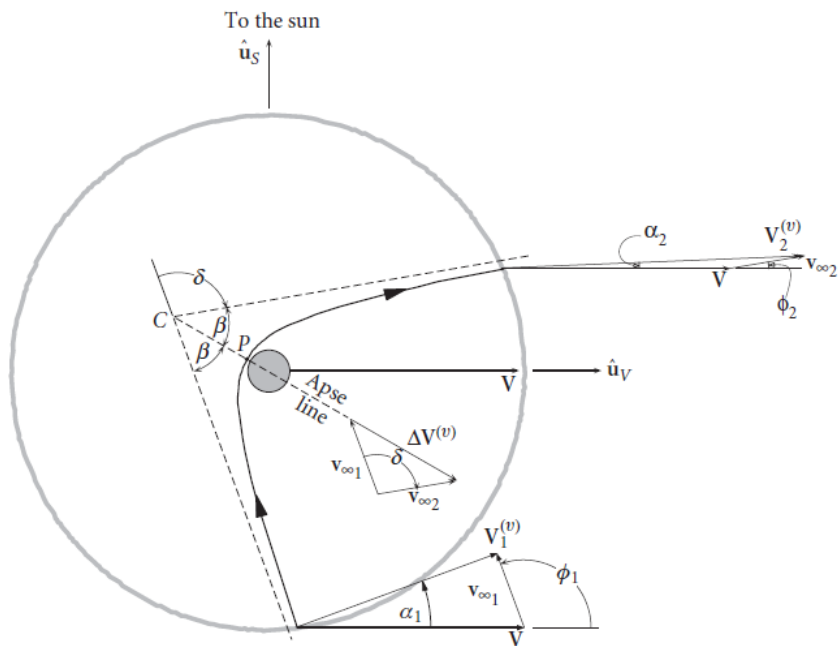


Figure 3.9: Trailing-side flyby [1]

3.5 Coordinate systems

The motion of a spacecraft around the Earth, or around another celestial body, is defined in a particular coordinate system. The different coordinate systems used in this document are described in the present section.

3.5.1 ECI system

ECI, Earth Centered Inertial, is a geocentric coordinate system, so it has the center of the Earth as origin, in which the equator represents the fundamental plane and the vernal equinox indicates the positive direction of the X axis.

ECI is a system fixed with respect to the stars (with only the precession of the equinoxes as exception), so it is called inertial, while the Earth rotates relative to it.

The apparent motion of the Sun viewed from Earth defines an orbit plane called the ecliptic, this is a different plane with respect to the Earth's equatorial plane. In fact an angle of $23^{\circ}27'$ is described between the two defined planes.

Two directions are used in order to define the orientation of an ECI frame: the orientation of the Earth's rotational axis in space and the ecliptic plane.

At the point where the Earth-Sun vector (directed from Earth to the sun) points at the intercept between the ecliptic and the celestial equator, an equinox is defined. The vernal equinox, which occurs near the first day of spring in the northern hemisphere (21 March), is used to indicate the direction of the X axis on the ECI frames.

As fundamental plane for the ECI frames the equatorial plane, or the ecliptic, can be used. In this document the first one is adopted.

The orientation of the X axis in this frame is not fixed over the time, mainly as a result of the combined effect of the Earth's asphericity and of the luni-solar gravitational effects, that produces a slowly moving of the ecliptic and of the celestial equator. This phenomenon is called precession and causes a continuous turning of the coordinate system westward relative to the poles of the ecliptic, a complete revolution is described in about 26000 years. Another effect, called nutation, generates a small oscillation of the Earth's axis with a period of 18.6 years (that is equal to the time of revolution of the nodes in the Moon's orbit).

The EME2000, or J2000, is a particular ECI frame determined with the Earth's Mean Equator and Equinox at 12:00 Terrestrial Time on 1 January 2000.

The X axis is aligned with the mean equinox. The Z axis is aligned with the Earth's spin axis or celestial North Pole. The Y axis is rotated by 90 degrees East about the celestial equator.

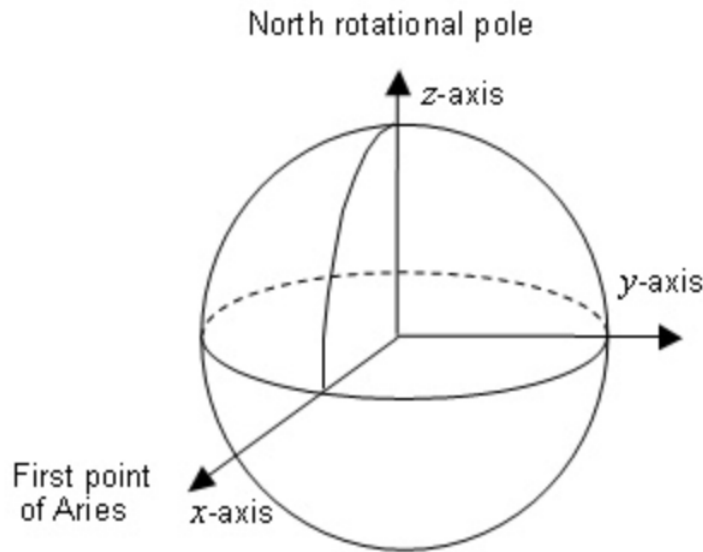


Figure 3.10: J 2000 ECI reference system [16]

3.5.2 Heliocentric system

The orbits of a spacecraft in the Solar System can be efficiently described by using an ecliptic heliocentric coordinate system. The use of ecliptic as fundamental plane is beneficial because most planets and many small Solar System bodies (for example asteroids) have orbits with slight inclinations with respect to this plane.

The system has its origin in the mass centre of the Sun, the primary direction (positive X values) is indicated by the vernal equinox. The Z axis is aligned with the celestial North Pole. It has a right-hand convention. Also in this case the EME2000, or J2000, is used to establish a fixed standard direction.

3.5.3 Spherical coordinates

In both the introduced coordinate systems, spherical coordinates (polar 3D coordinates) are used to identify the position of the generic point P as a function of the quantities (r, θ, ϕ) , which are defined as:

- radius, r , indicates the magnitude of the segment that connects the origin O and the point P (segment \overline{OP}). It is the distance between O and P.
- right ascension, θ , measures the angle between the X axis and the segment \overline{OQ} , where Q is the projection of P in the fundamental plane XY.

- declination, ϕ , measures the angle between the fundamental plane and the segment \overline{OP} .

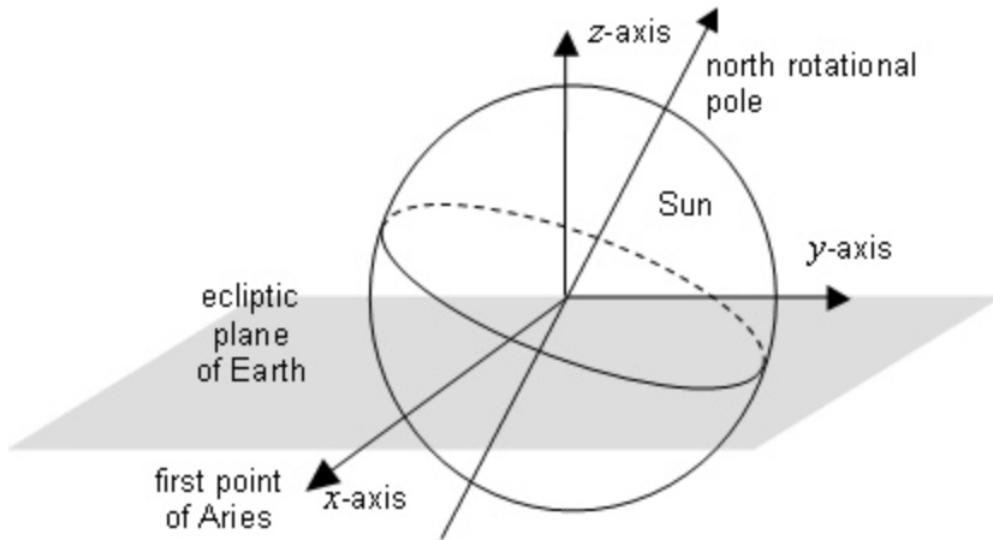


Figure 3.11: J 2000 heliocentric ecliptic reference system [16]

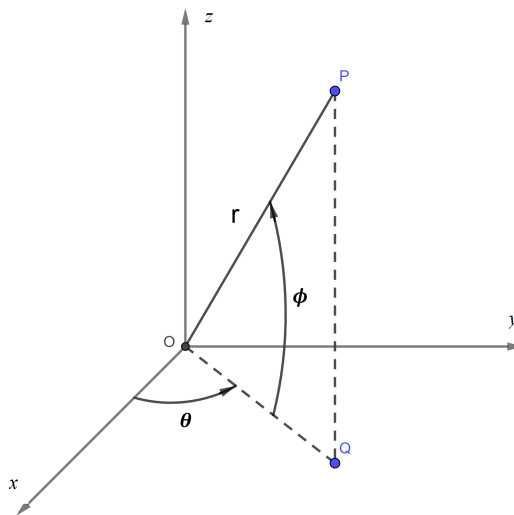


Figure 3.12: spherical coordinates

Analysis

Although the advent of private space companies causes market competition and consequently, a reduction of the costs, present-day launch costs of a space missions are still considerable. Regarding to low Earth orbit (LEO), they ranging from 2,500 to 25,000 dollars per kilogram. If launch can be made less expansive, the mission itself will be cheaper, taking into account that launch costs represents a large percentage of the cost of all space activities.

In this context, payload maximization is fundamental to reduce costs and to mission feasibility. Is possible to pursue these objectives through the use of numerical methods. Numerical methods for trajectory optimization can be in general classified into three main groups: indirect methods, direct methods, and evolutionary algorithms.

Indirect methods are typically faster and more accurate compared to direct methods (because of the reduced number of variables) and they can provides useful theoretical notions on the problem to be solved. However, the use of these techniques also involves drawbacks:

- it is required to derive analytic expressions for the necessary conditions
- the convergence region for a shooting algorithm may be quite small

4.1 Shooting method

For the reasons exposed an indirect method has been used to evaluate the spacecraft trajectory. Indirect methods are commonly used to solve a class of ordinary differential equation (ODE): the boundary value problems (BVP). Strictly speaking BVP has been solved by using the shooting procedures. The shooting methods solve numerically the BVP problem by reducing it into the initial value problem (IVP). Different trajectories were calculated until a trajectory that matches the desired boundary values was founded. This method allows to estimate the initial conditions.

In the current problem escape radius and escape velocity components are imposed as also the inclination at launch:

$$r_f, u_f, v_f, w_f, i_0$$

Number of parameters are the same of imposed conditions, so we have:

$$\theta_0, \phi_0, v_0, w_0, \Delta t$$

Note that initial radius is not parameter, while it is fixed at $r_0 = 1.0302$. That is the radius of initial parking orbit, a dimensionless value by using mean Earth radius. In fact all the quantities used in the shooting method are dimensionless:

- geocentric distances become dimensionless by using mean Earth radius

$$r_{conv} = 6378 \text{ Km}$$

- geocentric velocities become dimensionless by using circular orbit velocity at Earth's surface

$$V_{conv} = 7.9054 \text{ Km/s}$$

- geocentric times become dimensionless by using the reference time

$$t_{conv} = \frac{r_{conv}}{V_{conv}} = 806.811 \text{ s};$$

- heliocentric distances become dimensionless by using mean Earth-Sun distance

$$r_{convelio} = 1.496 * 10^8 \text{ Km}$$

- heliocentric velocities become dimensionless by using circular orbit velocity of the Earth around the Sun

$$V_{convelio} = 29.7847 \text{ Km/s}$$

- heliocentric accelerations become dimensionless by using

$$t_{convelio} = a_{convelio} = \frac{\mu_{sun}}{r_{convelio}^2} = 5.93 * 10^{-6} \text{ Km/s}^2$$

- heliocentric times become dimensionless by using the reference time

$$t_{convelio} = \frac{V_{convelio}}{a_{convelio} * 86400} = 58.1324 \text{ days}$$

A transformation from geocentric reference to heliocentric reference and vice versa is possible by using these quantities. For example, when the numerical code starts an heliocentric dimensionless time is read from an input file and it is immediately transformed in a geocentric dimensionless time by using:

$$t_{escape-geo} = \frac{t_{escape-elio} * t_{convelio} * 86400}{t_{conv}}$$

Trajectory was, initially, divided into two phases: a first that started at perigee (circular parking orbit) and ended at the first lunar flyby and a second one from first lunar flyby to the escape. In that manner the whole problem has a single solution, because the number of free parameters equals the number of conditions.

Subsequently, two additional inner phases were inserted to improving the numerical convergence. Therefore, the whole trajectory was split into four phases:

1. from perigee to the first lunar flyby;
2. from first lunar flyby to apogee;
3. from apogee to the second lunar flyby;
4. from second lunar flyby to escape.

Among which, there are three internal points, where the state variables are discontinuous or where constraints are imposed:

1. first periselenium;
2. apogee;
3. second periselenium.

Considering the internal points, for each one we add a parameter (time) and a condition (relative velocity perpendicular to vector (S/C - Moon) for the periselenium, $u = 0$ at the apogee).

This method made up of 4 phases is knowing as the *multiple shooting method*, where additional variables are added after apogee's passage and continuity of these variables are inserted as conditions.

The method solves an initial value problem in each of the smaller intervals, and imposes additional matching conditions to form a solution on the whole interval. The division into smaller intervals guarantees improvement on numerical stability over single shooting methods. So, on the whole, four IVP are solved, derived from the initial BVP. Furthermore, nonlinear constraints at both internal and external boundaries are imposed.

In general, these boundary conditions are grouped into a vector ψ :

$$\psi(x_{(j-1)_+}, x_{j-}, t_{(j-1)_+}, t_{j-}) \quad j = 1, \dots, n \quad (4.1)$$

where the j_{th} arc starts at $t_{(j-1)_+}$ and ends at t_{j-} (+ and - denote values just after and before point j).

The initial values of some of the variables are usually unknown, for this reason the solution is determined through an iterative process. Known $p^{(r)}$, the initial values at the r -th iteration, obtained through previous iteration, the equations shall be integrated along the whole trajectory, taking into account any discontinuities in the internal boundaries. Notes that $p^{(1)}$ is derived from the tentative solution. At the end of the integration the errors on the boundary conditions are calculated.

Each unknown parameter is in turn perturbed by a small amount δp ; the new IVP is solved, and the change of the errors on the boundary conditions $\delta\psi$ is evaluated. The choice of the perturbation step δp is important to achieve a proper evaluation of the sensitivity matrix. A rule of thumb suggests δp of the same order of the square root of the absolute tolerance used by the integrator ($10^{(-7)}$ in this application). So Newton's method is used to bring the errors to zero.

Considering only first order's terms, is possible to write:

$$\delta\psi = \left[\frac{\partial\psi}{\partial p} \right] \delta p \quad (4.2)$$

So, in order to delete errors on the boundary conditions (i.e. $\delta\psi = -\psi^r$, because of $\psi^{(r+1)} = \psi^{(r)} + \delta\psi = 0$), at each iteration the initial values are corrected as:

$$\delta p = p^{(r+1)} - p^{(r)} = \left[\frac{\partial\psi}{\partial p} \right]^{-1} \psi^r \quad (4.3)$$

until the boundary conditions are verified with the desired accuracy. In order to not get too far from the solution, only a fraction of the correction is made:

$$p^{(r+1)} = p^{(r)} + K_1 \delta p \quad (4.4)$$

where $K_1 = 0.1 - 1$, depending on how the attempt solution is distant from the solution sought.

At each iteration, after the evaluation of vector $p^{(r+1)}$ by using equation 4.4, the equations of the motion (described in the next section) are been integrated and a comparison between the maximum error on the boundary condition at the current iteration $E_{max}^{(r+1)}$ and the same error on the previous iteration $E_{max}^{(r)}$ is performed. If $E_{max}^{(r+1)} < K_2 E_{max}^{(r)}$ is possible to

proceed with the next iteration. K_2 coefficient is necessary because while convergence is sought the error may increase on the early steps.

$K_2 = 2 - 3$ typically represents a good choice.

Else if $E_{max}^{(r+1)} > K_2 E_{max}^{(r)}$ a bisection of the correction is performed and the equations of motion are been integrated with the attempt values:

$$p^{(r+1)} = p^{(r)} + \frac{K_1 \delta p}{2} \quad (4.5)$$

repeating the comparison between the two maximum errors ($E_{max}^{(r+1)}$ and $E_{max}^{(r)}$) and, if necessary, repeating the bisection. A maximum number of 5 bisections is fixed, after these the procedure has been arrested, meaning that the attempt solution is not appropriate to carry to the convergence.

An example of the vector $r^{(p)}$ is illustrated in figure 4.1, this is the solution obtained when the method reaches the convergence for the case A described in the next chapter.

	0	0	0	0	4	4
	4	4	4	4	4	4
	4	4	4	4	4	4
209.802316187610		5502.42668010828		11667.8240092373		
12537.3421251948						
1.000000000000000	331.819510413982		4.93839809107386			
-0.651469107185109	-3.667320641556965E-026		6.921270632789815E-003			
-3.875749661355688E-003	0.000000000000000E+000		0.000000000000000E+000			
0.000000000000000E+000	1.64399200517667		0.446121141583193			
-1.340021368109381E-025	1.35527391708683		0.314216126132073			
0.000000000000000E+000	1.000000000000000		0.000000000000000E+000			
0.000000000000000E+000	0.982219977597532					

Figure 4.1: example of $p^{(r)}$ vector

A brief description of the quantities contained in the $p^{(r)}$ vector is given.

The first 18 terms indicate the nature of the phase: 0 states for a coast phase (no thrust), 1 for a thrust phase, 4 denotes a phase that has to be ignored (no phase). In this case, four phases are identified.

Following, 4 terms indicate the time frames for the phases of the mission, starting from the perigee launch (they are identified as: t_1, t_2, t_3 and t_4).

After that, one term is set equal to 1 (fixed), followed by 6 terms, which represents position (r_2, θ_2, ϕ_2) and velocity (u_2, v_2, w_2) of the apogee.

Then, three terms are equal to zero and represents $\Delta\lambda_r, \Delta\lambda_\theta$ and $\Delta\lambda_\phi$ of the periselenium. From this fact descends an important condition: the radius of the periselenium is a free parameter.

Subsequently, since that r_0 is fixed, only 5 terms are used indicate the position and velocity of the perigee ($\theta_0, \phi_0, u_0, v_0, w_0$). Since that a topocentric reference frame is used, the radial velocity component at perigee and at apogee is null: $u_0 = u_2 = 0$.

Finally, 4 terms represent respectively: λ_{r_0} , λ_{u_0} , λ_{v_0} , λ_{w_0} , while the last one is the mass at the perigee launch m_0 . Considering that no propellant is used during the escape leg (which is a coast phase), mass at perigee m_0 is equal to the escape mass m_∞ . It is evaluated by using the method that will be explained later.

4.2 Equation of motion

The spacecraft is modeled as a point with variable mass. Position \bar{r} , velocity \bar{v} , and mass m of the spacecraft are the problem's state variables, described by differential equations:

$$\begin{cases} \frac{d\bar{r}}{dt} = \bar{v} \\ \frac{d\bar{v}}{dt} = -\frac{\mu\bar{r}}{r^3} + \frac{\bar{T}}{m} + \bar{a}_P \\ \frac{dm}{dt} = -\frac{T}{c} \end{cases} \quad (4.6)$$

where $-\frac{\mu\bar{r}}{r^3}$ is the spherical-Earth gravitational acceleration, \bar{a}_P collects the perturbing accelerations due to Earth's oblateness \bar{a}_J , to Moon and Sun attraction \bar{a}_{lsg} , and to solar radiation pressure \bar{a}_{srp} .

$$\bar{a}_P = \bar{a}_J + \bar{a}_{lsg} + \bar{a}_{srp} \quad (4.7)$$

The thrust vector \bar{T} is assumed to be zero in the present document (all the phases are coasted).

It is adopted the EME2000 reference frame (Earth Mean Equator and Equinox of Epoch J2000): \hat{I} , \hat{J} , and \hat{K} are unit vectors along the axes of EME2000. Precession and nutation are neglected. The position is expressed in spherical coordinates by using: radius r , right ascension θ and declination ϕ :

$$\bar{r} = r \cos\theta \cos\phi \hat{I} + r \sin\theta \cos\phi \hat{J} + r \sin\phi \hat{K} \quad (4.8)$$

A topocentric reference frame is introduced, whose unit vectors are \hat{i} (radial), \hat{j} (eastward), and \hat{k} (northward).

$$\begin{Bmatrix} \hat{i} \\ \hat{j} \\ \hat{k} \end{Bmatrix} = \begin{bmatrix} \cos\theta \cos\phi & \sin\theta \cos\phi & \sin\phi \\ -\sin\theta & \cos\theta & 0 \\ -\cos\theta \sin\phi & -\sin\theta \sin\phi & \cos\phi \end{bmatrix} \cdot \begin{Bmatrix} \hat{I} \\ \hat{J} \\ \hat{K} \end{Bmatrix} \quad (4.9)$$

In the topocentric frame the position vector can be easily written as $\bar{r} = r\hat{i}$, while the velocity as

$$\bar{v} = \dot{\bar{r}} = u\hat{i} + v\hat{j} + w\hat{k} \quad (4.10)$$

where u, v, and w being radial, eastward, and northward components, respectively.

Then the scalar state equations can be derived:

$$\left\{ \begin{array}{l} \frac{dr}{dt} = u \\ \frac{d\theta}{dt} = \frac{v}{r \cos \phi} \\ \frac{d\phi}{dt} = \frac{w}{r} \\ \frac{du}{dt} = -\frac{\mu}{r^2} + \frac{v^2 + w^2}{r} + \frac{T_u}{m} + (a_P)_u \\ \frac{dv}{dt} = \frac{(-uv + vw \tan \phi)}{r} + \frac{T_v}{m} + (a_P)_v \\ \frac{dw}{dt} = \frac{(-uv + v^2 \tan \phi)}{r} + \frac{T_w}{m} + (a_P)_w \\ \frac{dm}{dt} = -\frac{T}{c} \end{array} \right. \quad (4.11)$$

Is important to not forget that the thrust and all her components are assumed to be zero along the whole trajectory of escape.

4.3 Perturbations

In this document the following perturbations will be included:

- perturbation due to the Earth asphericity;
- perturbation due to the gravitational attraction of the Sun;
- perturbation due to the gravitational attraction of the Moon;
- pressure of solar radiation.

Also the eccentricity of Moon's orbit is taking into account.

4.3.1 Earth asphericity

In order to evaluate the effects of the Earth's oblateness, a description of the Earth potential based on the Earth Gravitational Model EGM2008 is used. This method provides normalized spherical harmonic coefficients for the Earth gravitational potential; the “Tide Free” system is used (which means that all direct and indirect, effects of the Sun and Moon are removed). A uniform rotation of the Earth is assumed, while precession and nutation are neglected. The EME2000 reference frame is adopted.

Using this formulation the potential corresponding to the Earth asphericity can be written as:

$$\Phi = -\frac{\mu_E}{r} \sum_{n=2}^N \left(\frac{r_E}{r}\right)^n \sum_{m=0}^n (C_{nm} \cos(m\lambda) + S_{nm} \sin(m\lambda)) P_{nm}(\sin\phi) \quad (4.12)$$

where r_E is the semi-major axis of the Earth ellipsoid. $N = 8$ is used in this document. The associated Legendre functions $P_{nm}(\sin\phi)$ and the spherical harmonic coefficients C_{nm} and S_{nm} are taken in the unnormalized form that permits faster computations. Normalized quantities would allow for a greater accuracy, which is not necessary for the present application.

The declination ϕ corresponds to the terrestrial latitude, while terrestrial longitude λ is obtained as $\lambda = \theta - \theta_{Gref} - \omega_E(t - t_{ref})$ where θ_{Gref} is the Greenwich right ascension at the reference time t_{ref} .

The perturbing acceleration due to the Earth asphericity is the gradient of $-\Phi$, and its components in the topocentric frame are thus evaluated as :

$$\begin{cases} (a_J)_u = -\frac{\partial\Phi}{\partial r} \\ (a_J)_v = -\frac{(\partial\Phi/\partial\theta)}{r \cos\phi} \\ (a_J)_w = -\frac{(\partial\Phi/\partial\phi)}{r} \end{cases} \quad (4.13)$$

derivatives with respect to ϕ require the derivatives of the associated Legendre functions, which are obtained recursively.

4.3.2 LuniSolar perturbation

The lunisolar perturbation is given by the sum of the gravitational perturbations due to the Moon and to the Sun. Positions of Sun and Moon are evaluated by DE405 JPL ephemeris. It gives the body position in rectangular coordinates x_b , y_b and z_b with respect

to the Earth in the International Celestial Reference Frame and therefore in the EME2000 frame (between these frames there are very small differences that can be neglected in the present problem). Subscript b could indicates the Sun (b=s) or the Moon (b=l).

The perturbing acceleration on the spacecraft

$$\bar{a}_{bg} = -\left(\frac{\mu_b}{R^3}\right)\bar{R} - \left(\frac{\mu_b}{r_b^3}\right)\bar{r}_b \quad (4.14)$$

is caused by a body with gravitational parameter μ_b , whose position vector relative to the Earth is: $\bar{r}_b = x_b\hat{I} + y_b\hat{J} + z_b\hat{K}$, where $\bar{R} = \bar{r} - \bar{r}_b$ is the spacecraft relative position vector with respect to the perturbing body and $-\bar{r}_b$ is the Earth relative position, as can be seen in Figure 4.2.

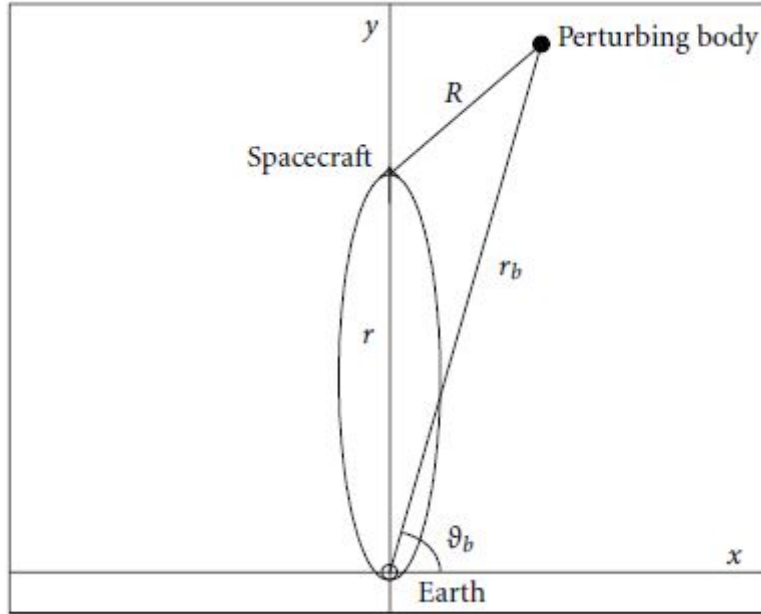


Figure 4.2: Schematic geometry of gravitational perturbations [8]

The perturbing acceleration is not composed only by the gravitational acceleration that the perturbing body causes on spacecraft, but also on the Earth. In the topocentric frame (based on the spacecraft position), it can be written as

$$\begin{cases} (\bar{a}_{bg})_u = \left(\frac{\mu_b}{R^3}\right)[(r_b)_u - r] - \left(\frac{\mu_b}{r_b^3}\right)(r_b)_u \\ (\bar{a}_{bg})_v = \left(\frac{\mu_b}{R^3}\right)(r_b)_v - \left(\frac{\mu_b}{r_b^3}\right)(r_b)_v \\ (\bar{a}_{bg})_w = \left(\frac{\mu_b}{R^3}\right)(r_b)_w - \left(\frac{\mu_b}{r_b^3}\right)(r_b)_w \end{cases} \quad (4.15)$$

with

$$R = \sqrt{[r - (r_b)_u]^2 + (r_b)_v^2 + (r_b)_w^2} \quad (4.16)$$

The position components of the perturbing body "b" in the spacecraft topocentric frame are:

$$\begin{cases} (r_b)_u = x_b \cos \theta \cos \phi + y_b \sin \theta \cos \phi + z_b \sin \phi \\ (r_b)_v = -x_b \sin \phi + y_b \cos \theta \\ (r_b)_w = -x_b \cos \theta \sin \phi - y_b \sin \theta \sin \phi + z_b \cos \phi \end{cases} \quad (4.17)$$

4.3.3 Solar radiation pressure

For this perturbation, it must be taken into consideration the photon pressure: at a distance R from the Sun, it can be evaluated as:

$$p = \frac{L_s}{4\pi R^2 c_{light}} \quad (4.18)$$

where L_s is the total power radiated by the Sun and c_{light} is the speed of light. At a distance $R = 1 \text{ AU}$, $p = 4.55682 * 10^{(-6)} \text{ N/m}^2$. The acceleration on a spherical body is

$$\bar{a}_{srp} = (1 + \eta) p^* \left(\frac{R^*}{R} \right)^2 \left(\frac{S}{m} \right) \frac{\bar{R}}{R} = \frac{\Gamma \bar{R}}{m R^3} \quad (4.19)$$

with the cross-section "S", the mass of the spacecraft "m" and the reflectivity " η ". Projected onto the topocentric frame:

$$\begin{cases} (a_{srp})_u = \left(\frac{\Gamma}{m R^3} \right) [(r_s)_u - r] \\ (a_{srp})_v = \left(\frac{\Gamma}{m R^3} \right) [(r_s)_v] \\ (a_{srp})_w = \left(\frac{\Gamma}{m R^3} \right) [(r_s)_w] \end{cases} \quad (4.20)$$

Since the solar radiation pressure acts along the Sun-spacecraft direction, this acceleration is parallel but with opposite directions to the solar gravity acceleration and also is inversely proportional to the squared distance of the two bodies. In the equation 4.19 it can be noted that, unlike equation 4.14, the perturbing acceleration depends on the instantaneous mass.

4.4 Mass evaluation

Finally, the model that gives the escape mass evaluation is illustrated.

The values of position and velocity at perigee (V_P) are rotated to the J2000 ECI frame to determine the corresponding latitude, longitude and azimuth. Azimuth and $\Delta V_P = V_P - V_C$ can be used to evaluate the mass that the launcher can insert into the escape trajectory.

The following calculations refer to the Delta IV Heavy rocket. The starting mass on the initial 200-km parking orbit is the sum of useful mass (m_u) and upper stage dry mass m_d (3550 kg). The useful mass given by NASA's Launch Vehicle Performance Website is here approximated with the quadratic equation:

$$m_u = 26280 - 0.6642(A - 90)^2 \quad (4.21)$$

where m_u is in kg and the azimuth A in degrees. Rocket equation can be used to evaluate the useful escape mass:

$$m_\infty = (m_u + m_d)e^{\left(\frac{-\Delta V}{c}\right)} - m_d - m_{PAF} \quad (4.22)$$

where the stage dry mass and the payload attach fitting mass (800 kg) are subtracted from the final mass. In addition:

$$\Delta V = 1.046(V_P - V_{P0}) \quad (4.23)$$

where V_P is the perigee velocity at the start of the trajectory to the Moon, and V_{P0} is the circular velocity of the parking orbit. An addition of a 4.6 % margin is included to attain a reference value of 9995 kg for the escape mass in the case of $C_3 = -1.5 \text{ km}^2/\text{s}^2$.

Features of the mission

5.1 interplanetary leg: the ARM mission

Lunar gravity assist maneuvers are used to reach the escape conditions needed to accomplish the desired space mission. They are useful because allow to increase the escape mass, in which payload mass is included, with a fixed energy of escape (due to a gain of ΔV without using propellant, as illustrated previously).

A double lunar gravity assist was planned to be employed in the scientific mission firstly presented by NASA in 2013: the ARM mission.

The Asteroid Redirect Mission (ARM) proposed to reach a large Near-Earth asteroid in order to pick up a heavy boulder (2-3 m of diameter) from its surface and to bring it into a lunar stable orbit. Thereafter, manned missions would have been directed to the boulder, with the purpose of exploring it and collecting samples for a detailed analysis on Earth.

The entire mission represents a testing ground for new technologies and spaceflight experience which will be useful for the future manned missions directed to the Moon and to Mars.

In order to identify the best candidate, NASA's Near-Earth Object Observation Program has discovered more than 1000 new near-Earth asteroids, among which four of them could be good candidates for the ARM. Target of the mission is chosen by NASA's scientists by evaluating orbit, velocity, size and spin of the different asteroids.

The carbonaceous boulder that would have been redirected by the mission (maximum 6 meter diameter, 20 tons) is not big enough to harm our planet because, despite it entering Earth's atmosphere, it would burn up. Bringing the asteroid boulder to a distant retrograde orbit around the Moon would ensure it could not encounter the Earth and also it is leaved in a stable orbit, suitable for future studies.

NASA paid their attention on 2008 *EV₅* as a preliminary baseline target. Itokawa, Bennu and several other asteroids, were considered besides 2008 *EV₅*, indeed no definitive choices have been operated.

2008 EV_5 is an oblate spheroid with a diameter of 400 m (sub-kilometer asteroid). This celestial body rotates in a retrograde direction with a very low speed. A 150 m diameter concave feature was observed on the asteroid, it can represent an impact crater, or a reconfiguration of the asteroid's shape caused by an episode of rapid rotation in the past. Visible and near-infrared spectroscopy highlight a composition which is similar to that of carbonaceous chondrite meteorites.

2008 EV_5 is part of the Aten group (a group of near-Earth asteroids which have a semi-major axis smaller than 1 AU and with an high eccentricity), and it was discovered on 4 March 2008.

The asteroid is characterized by: a semi-major axis of 0,958242 AU, an eccentricity of 0,083401 and an inclination of 7,437 degrees. On 23 December 2008, 2008 EV_5 made a close approach to Earth at a distance of 3.2 million km (0,022 AU), its closest until 2169. It is potentially hazardous to our planet, which means that the asteroid has an orbit that can make exceptionally close approaches to the Earth and it is large enough to cause significant regional damage if an impact occurs.

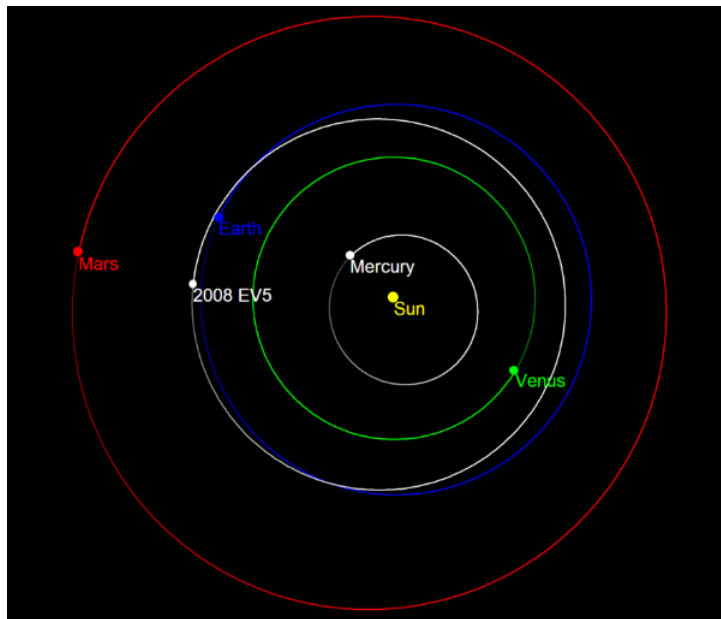


Figure 5.1: Orbit of 2008 EV_5 (in white), position on 1st January 2010 [18]

Unfortunately, the development of the Asteroid Redirect Mission ended under a directive of the White House, in December 11, 2017, that establishes the defunding and so the consequently closeout of the mission. Nevertheless, many of the central technologies in development for that mission, such as solar electric propulsion, will continue, as they constitute vital capabilities needed for future human deep space missions. Also the implementation of a double LGA may be useful with the perspective of similar missions.

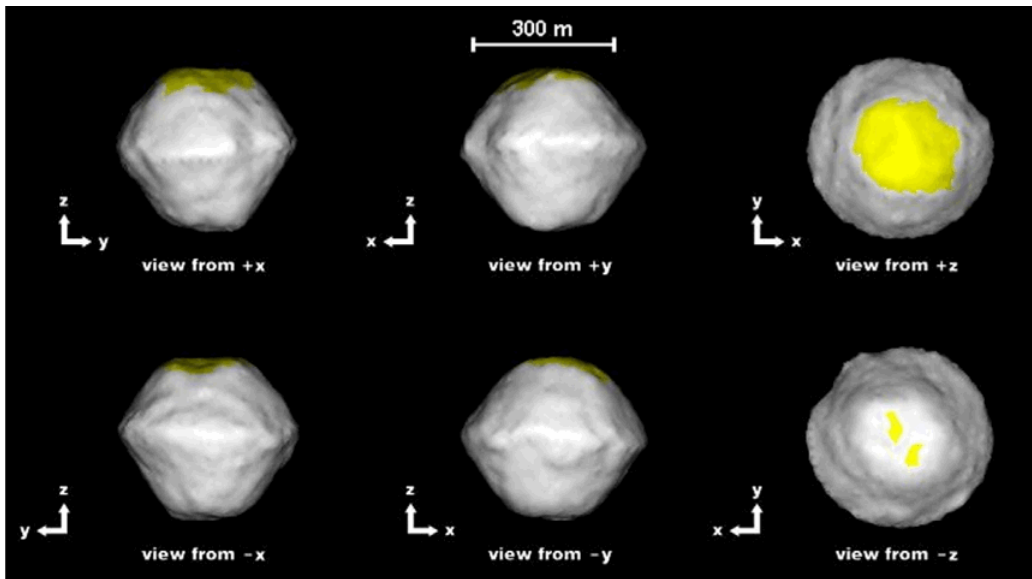


Figure 5.2: different views of the 2008 EV₅ [18]

5.2 Solar perturbed Moon to Moon leg

As long as a preliminary analysis of an interplanetary mission can be conducted by employing the patched conic approximation, escape phase and heliocentric phase can be studied separately.

Two different approaches can be used when lunar gravity assist (LGA) escape trajectories have to be designed.

The first one pre-computes and maps the escape C_3 (which is the hyperbolic escape energy, defined as $C_3 = V_\infty^2$, in km^2/s^2) as a function of date (i.e., position of the Moon along its orbit) and C_3 value before the flyby.

In the other approach, the interplanetary leg is first evaluated, then the trajectories to the target celestial body are computed for different departure dates and values of hyperbolic excess velocity. Indirect methods can perform this analysis in a reduced computational time. For each trajectory, feasibility and performance of a LGA escape are evaluated by means of an approximate analysis that may also provide tentative solutions for a detailed analysis of the maneuver.

Short maneuvers, which are supposed to be less affected by solar perturbation, are treated with the approximate analytical approach. On the other hand, during longer Moon to-Moon transfers an evaluation of the pre-computed C_3 is used to analyze planar escape sequences. In this manner is possible to take into account the relevant effects of the solar perturbation on the escape trajectory.

In this document a result that descends from the first of the two approaches is applied as a reference solution, guiding through the implementation of the numerical solution. It is explained in detail in the next chapter.

Only maneuvers with two lunar gravity assists are considered in this analysis. The development of solar-perturbed trajectories that connect two lunar flybys is challenging because these trajectories are no longer simply conic, so a pre-computed database of Moon-to-Moon transfers in the Sun-Earth CRTBP (circular restricted three body problem) covers the phase between two lunar encounters.

An upper case letter indicates the number of lunar revolutions (in an approximated way) between the two lunar flybys, therefore first letter of each family name denotes the time frame using alphabetic order. In such a manner is possible to group lunar-lunar transfers in different families.

Additionally, two lowercase letters, "o" and "i", follow the uppercase letter and identify the kind of flybys, which can be outbound or inbound.

As the solar phase angles varying, significant differences between trajectories of the same family can be noted.

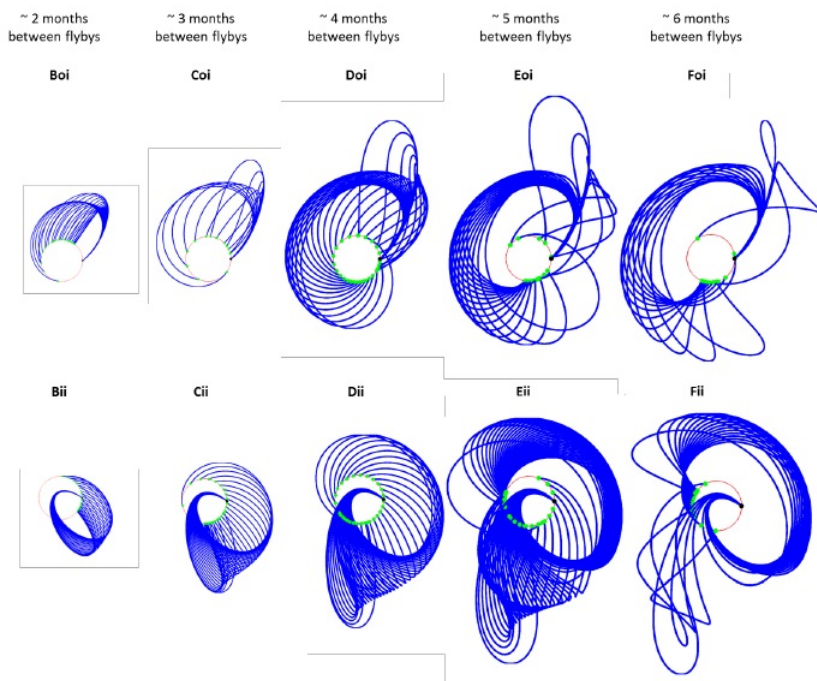


Figure 5.3: Families of solar-perturbed Moon-to-Moon transfers for an initial lunar relative velocity of 1 km/s. The Moons initial and final positions at the flybys are identified by black and green dots, respectively. Each family includes various trajectory that correspond to a different solar phase angle. To visually emphasize the differences between family members, all trajectories are rotated so that can start at the same lunar position [6]

In the case of an out of plane escape, the flyby event has also to provide a turn angle capable of both boost the energy of the spacecraft and change the plane of the trajectory, meaning that the out of plane scenarios cannot reach the values of C_3 that the in plane ones do. A relation between the declination of the escape, i.e. its inclination with respect to the Earth's ecliptic plane, and the maximum achievable C_3 , exists.

As can be seen in Figure 5.4 an escape C_3 up to $1.5 \text{ km}^2/\text{s}^2$ is guaranteed for any right ascension and declination directions. The escape C_3 tapers off in a more gradual way if compared to the results obtained by using two-body approximation only.

As is possible to predict, the maximum escape C_3 decreases with increasing declination, since flyby is most effective when V_∞ vector of the spacecraft is aligned with the orbital velocity vector of the encountered body.

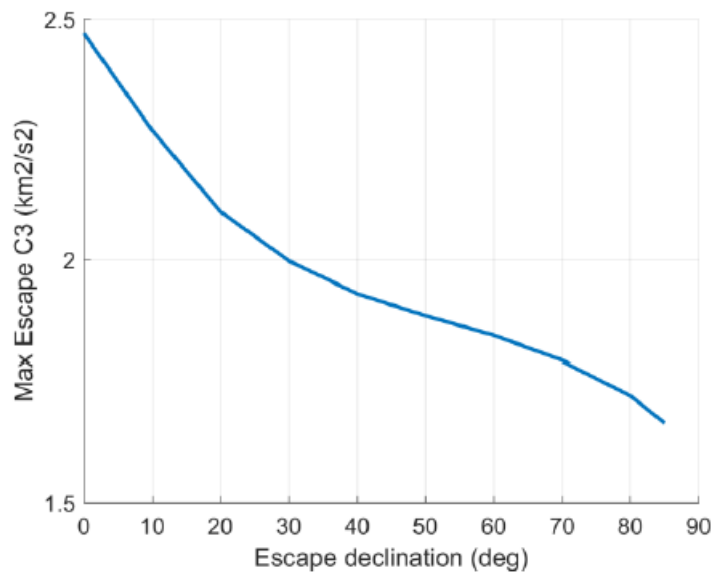


Figure 5.4: Maximum escape C_3 vs declination when lunar-assisted escape is used [6]

Results

Starting from the escape data and velocity necessary to accomplish the ARRM mission, the exact numerical solution of the escape maneuver is sought. It has to take into account the real ephemeris and the full gravity of the Sun, the Earth and the Moon.

Is possible to obtain the required input escape quantities by using MALTO (Mission Analysis Low Thrust Optimizer), a software tool for preliminary design of low-thrust trajectories, as a first optimizer and an indirect method for the further optimization steps (to produce a fully continuous trajectory). In such a manner, it has been evaluated that an escape in June 2022 with an inclination of -65° should be the optimal choice.

With regards to this thesis, the object is to design the escape leg. The entire phase is computed by using the multiple shooting method presented previously.

In order to reach the convergence of the numerical solution, is mandatory to proceed by steps, using a sequential target, for example the first flyby represents the initial target. Also a reference solution similarly to the present objective is required : a solution that pre-calculates the hyperbolic escape energy, C_3 , as a function of its value before the flyby event and of the date, can fulfill this task.

It was decided to use as reference solution an escape maneuver presented in the paper: "Design of Lunar-Gravity-Assisted escape maneuvers" by Lorenzo Casalino and Gregory Lantoine. It is illustrated in figure 6.1 and 6.2.

Starting from an attempt of replicate this solution is possible to investigate for other solutions that achieve the same escape condition by performing the two lunar flybys. Particular attention is placed on the final mass of escape and on the different escape velocity values.

Because of the different escape conditions that they involve, a crucial part of the escape maneuver is represented by the choosing of the Lunar-Lunar leg type. By analyzing the characteristics of the different families of transfer reported in figure 5.3, the authors chose a Moon to Moon transfer orbit of the Doi family.

Through successive optimization steps, the entire trajectory has been defined and it involves: the first flyby, which occurs on the 21st of February 2022 and the second flyby

on the 9th of June 2022 at an altitude of, respectively, 5119 km and 55 km, and with a Moon-relative velocity vector of 1.05 km/s in the first case and 2.15 km/s for the second case. The produced escape C_3 is 1.74 km²/s² with an ecliptic declination of -67.6°.

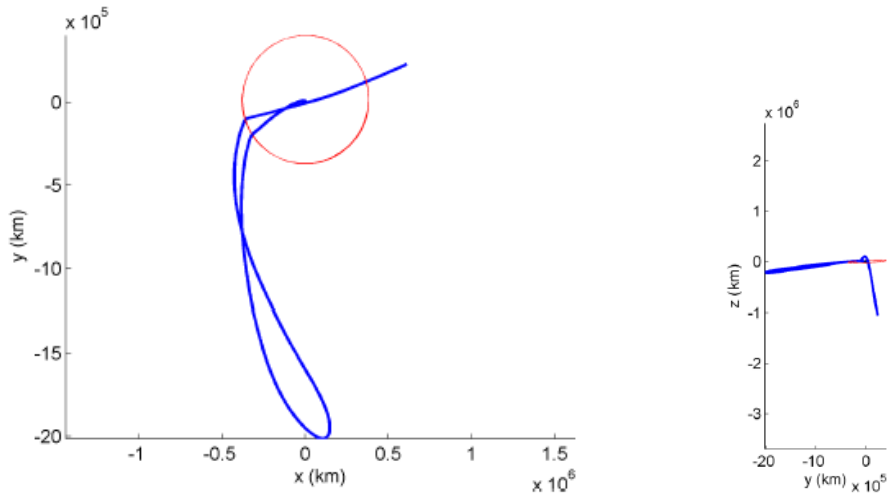


Figure 6.1: in plane and out of plane views of the reference solution in the ecliptic inertial reference frame [6]

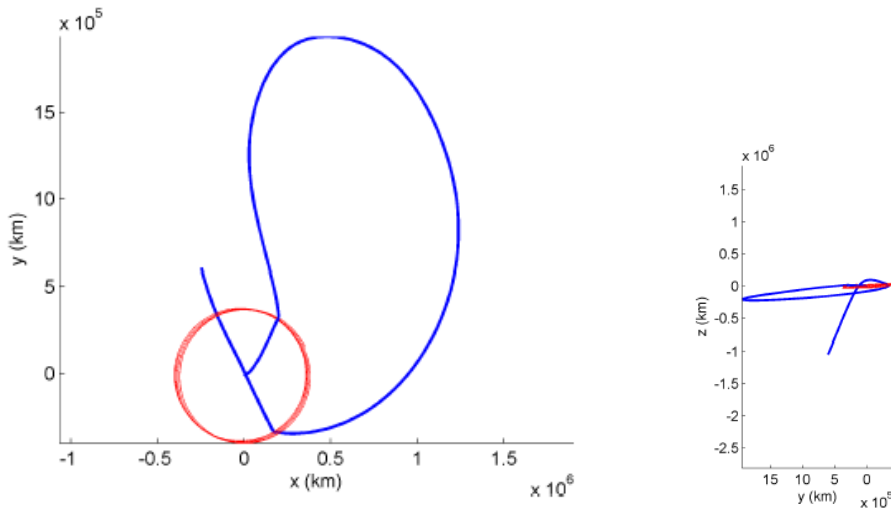


Figure 6.2: in plane and out of plane views of the reference solution in the Sun-Earth rotating frame [6]

6.1 Stepped procedure

Defined the reference solution is possible to start the analysis with the multiple shooting method by fixing the escape data and the heliocentric velocity, which are contained in an input file. All the dates reported from here on are related to the year 2022.

Knowing the final time of escape, on June 16, and setting an attempt solution which has a duration of 118 days, is possible to insert mission's starting time, that correspond to the 18th of February.

At this point, a solution that realizes the corrected first flyby, three days after the launch from the circular parking orbit (LEO), is sought by varying the angle θ_0 and ϕ_0 of the launch. Current target is to realize a first flyby with an angle $\theta < \theta_{Moon}$ (at the periselenium, in the geocentric reference frame), which is a trailing side flyby that allows the spacecraft to gain geocentric velocity.

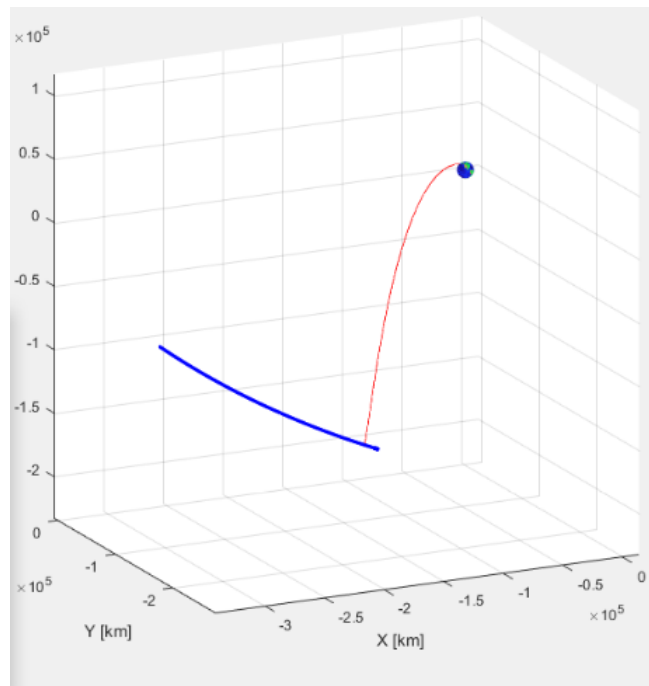


Figure 6.3: First flyby of the Moon, the red line identifies the spacecraft trajectory, the blue line identifies Moon's path

The next target is to perform a Moon to Moon leg that allows to realize a second flyby of the Moon. Reaching a distance from Earth similarly to the corresponding value in the reference solution and evaluate the effect of the solar perturbation that affects the spacecraft, are the critical points of this phase.

The orbital parameters, particularly the semi-major axis and the inclination, can give us these information. A change in inclination of 180° -(starting inclination value) causes the orbit to become a retrograde orbit. On the other hand the semi-major axis has to follow a declining trend, because of the solar gravity that pulls the spacecraft in the opposite direction of the current motion.

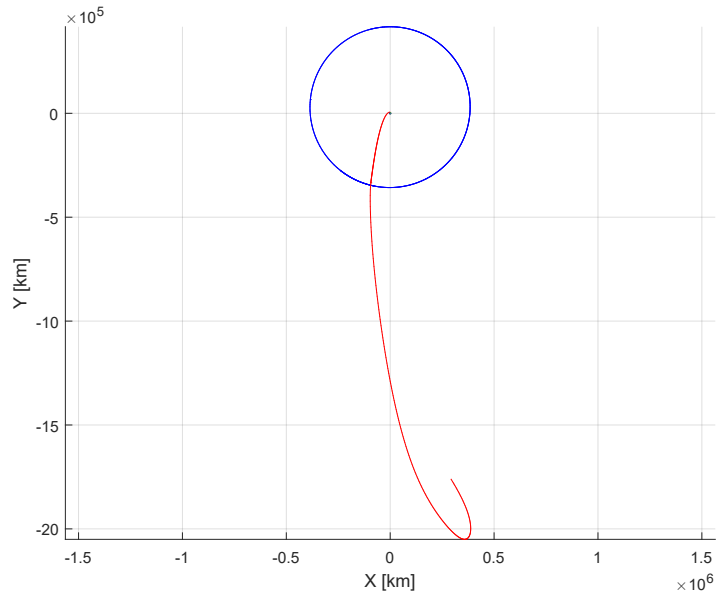


Figure 6.4: effect of the solar perturbation on the orbit

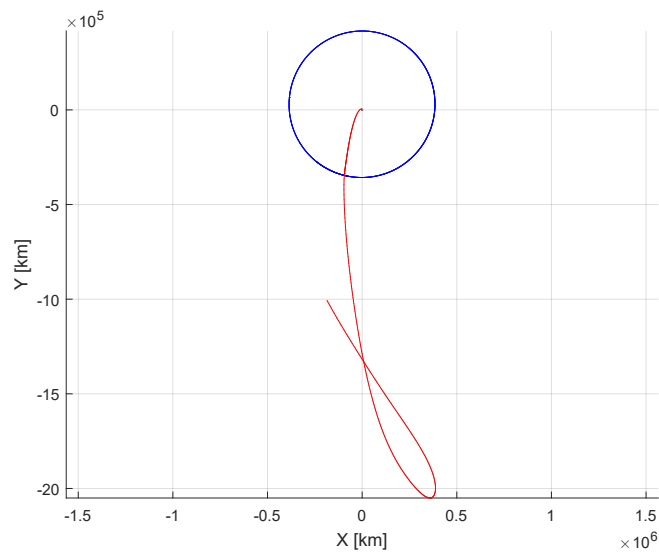


Figure 6.5: effect of the solar perturbation on the orbit

Last target is to achieve the required escape conditions by realizing the second lunar flyby. Because of the declination desired value at the escape and considering a Moon to Moon leg as a near planar transfer (almost lies in Moon's plane orbit) another trailing side flyby takes place, but this time it involves also a change in inclination. The spacecraft passes "under" Moon's orbit at the periselenium and this causes an initial increase of declination followed by a reduction that leads to the correct final value of -67.6° .

Shooting procedure achieving the convergence with a first flyby on the 23rd of February at a relative distance of 24725 Km (which corresponds to an altitude of 22988 Km above lunar surface, giving a Moon's radius of 1737 Km) and a second flyby that takes place on the 10th of June with a relative distance of 1796 Km from the Moon (it means a passage at an altitude of only 59 Km above lunar surface). One can notes that the first flyby in figure 6.3 is effectuated at lower distance with respect to that one in the complete solution. This is because the numerical code starts from an attempt solution and achieves a target by adjusting, iteration by iteration, the attempt solution.

The escape occurs on 18th of June, while launch from perigee is on 21st of February. Therefore, the mission has a duration of 117 days, very close to the 118 days of the reference mission.

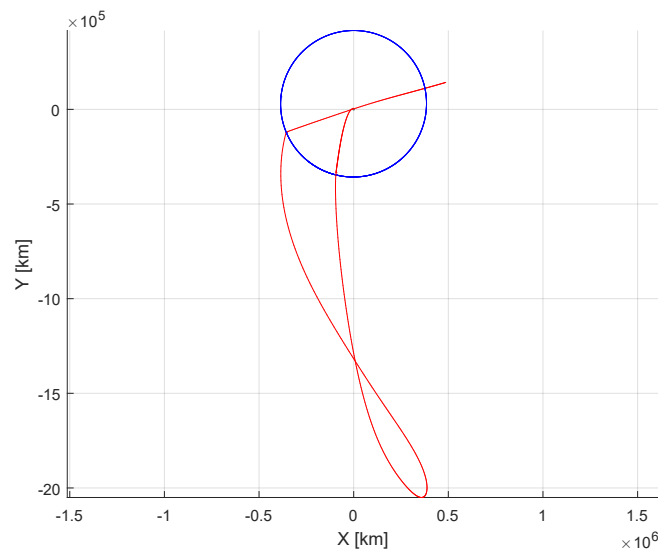


Figure 6.6: case A, escape on the 18th of June, XY view

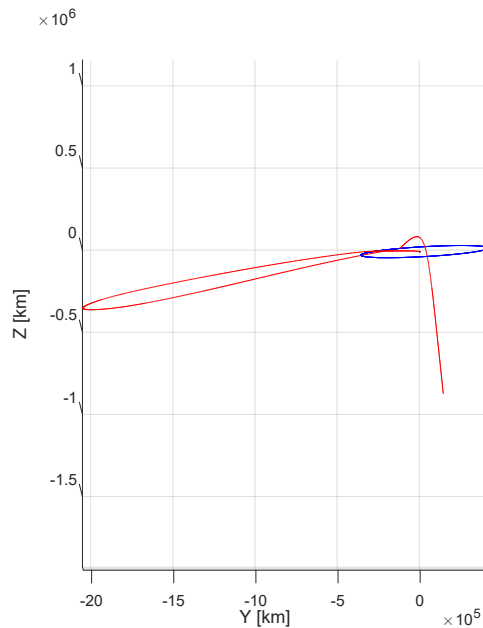


Figure 6.7: case A, escape on the 18th of June, YZ view

Finally, the steps to perform a solution are summarized:

- insert escape date on the input file "escape.txt" (code starts from this information and calculates backward the required time frame)
- achieve the right semi-axis and inclination (relative position to Earth and Sun) after first flyby – first flyby with an angle $\theta < \theta_{Moon}$ (trailing side flyby, accelerate the spacecraft and rises the apoapsis)
- realize a second flyby of the Moon which gives the correct escape position and velocity. It is obtained by adjusting Moon's relative position and velocity of the spacecraft at the first flyby

6.2 Cases with different data and escape velocity

Once that a solution is achieved, is possible to investigate the effect of a different time of escape. Whereas the constraint of the interplanetary mission persists and considering the quite difficult convergence of the code, escape data has been varied, directly in the input file, by a time step of 1 day to obtain case B and C and by a time step in the order of just half an hour (or less in some subcases) regarding to case D.

Case B is a solution which has a perigee launch on the 20th of February. The escape occurs on 17th of June and the flybys are respectively on the 22nd of February with a

periselenium of 33248 Km and on the 9th of June with an altitude of 1775 Km (that means an altitude of 38 Km above the surface). In order to reach a restrained error also a change in the escape velocity has been necessary, in particular a reduced value is required, passing from 1.61 Km/s to 1.55 km/s.

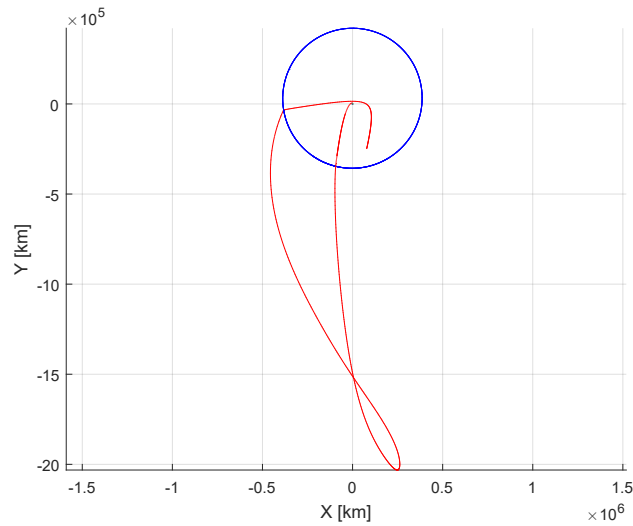


Figure 6.8: case B, escape on the 17th of June 2022, XY view

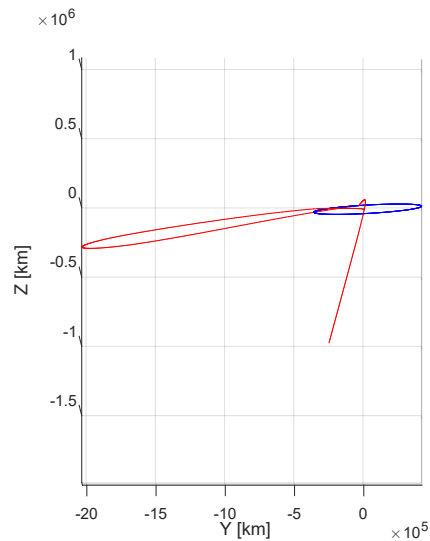


Figure 6.9: case B, escape on the 17th of June 2022, YZ view

Case C is a solution which has a launch on 22nd of February , while the 24th of February, at a distance of 21768 Km, and on the 10th of June, at a distance of 1887 Km, take place the two flybys. The escape maneuver reaches the target position on the 19th of June and, also in this case, a velocity change is required due to convergence necessity. The escape velocity has slightly augmented at the value of 1.56 Km/s.

An important difference exists between this case and the previously other: the first lunar flyby becomes a leading edge flyby, instead of a trailing edge one. This means that the spacecraft is no longer accelerated in the first lunar encounter, but a deceleration is verified. Figure 6.12 shows a detail of the first flyby.

Although the effect on the spacecraft is mitigate by a relative high distance with the Moon (more than 20000 Km among this three cases), and considering also that a higher apogee is reached in this case (see table 6.1), a higher launch velocity (from parking orbit) is needed. In fact a rise, from a value of 10.994 Km/s of the case B to a value of 11.025 Km/s for this case, can be noted by analyzing the $p^{(r)}$ vector.

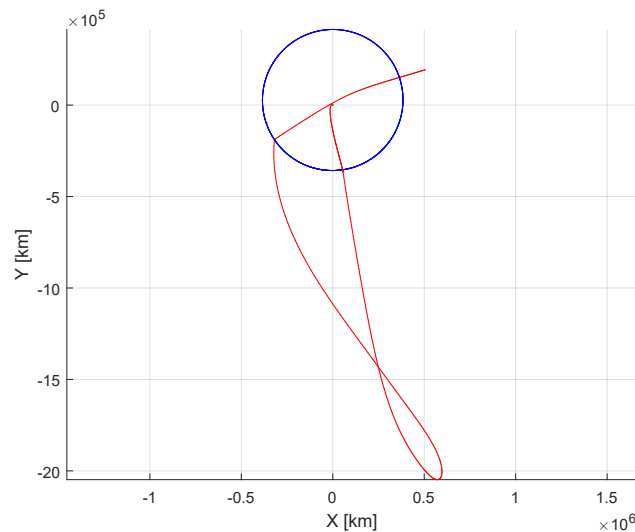


Figure 6.10: case C, escape on the 19th of June 2022, XY view

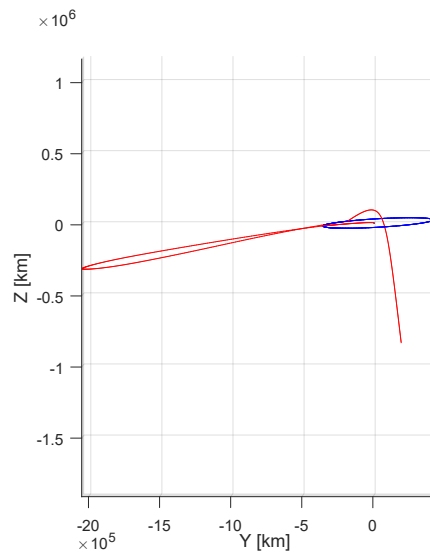


Figure 6.11: case C, escape on the 19th of June 2022, YZ view

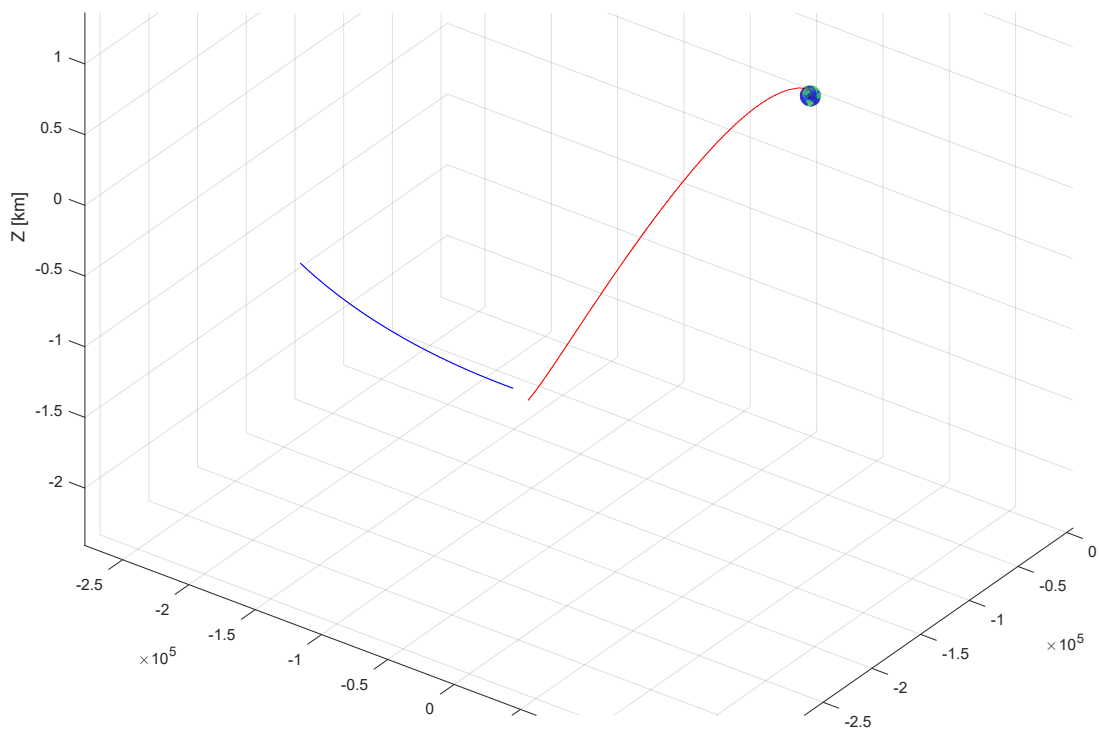


Figure 6.12: case C, a detailed view of the first flyby

Finally, case D is characterized by an escape on the 20th of June, obtained by moving the launch date on the 28th of February and the flybys on the 2nd March, with a distance of 2191 Km, and on the 11th of June, at a distance of 2496 Km. Another reduction in the escape velocity is needed at the value of 1.49 Km/s.

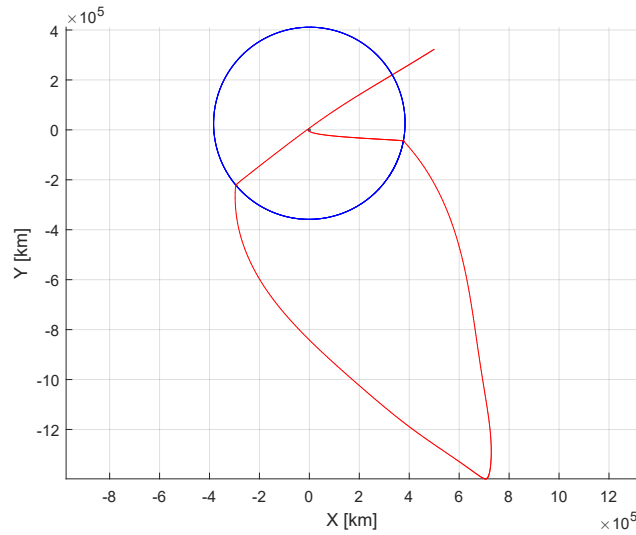


Figure 6.13: case D, escape on the 20th of June 2022, XY view

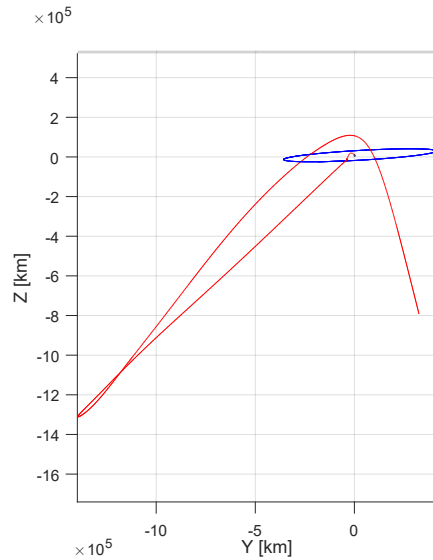


Figure 6.14: case D, escape on the 20th of June 2022, YZ view

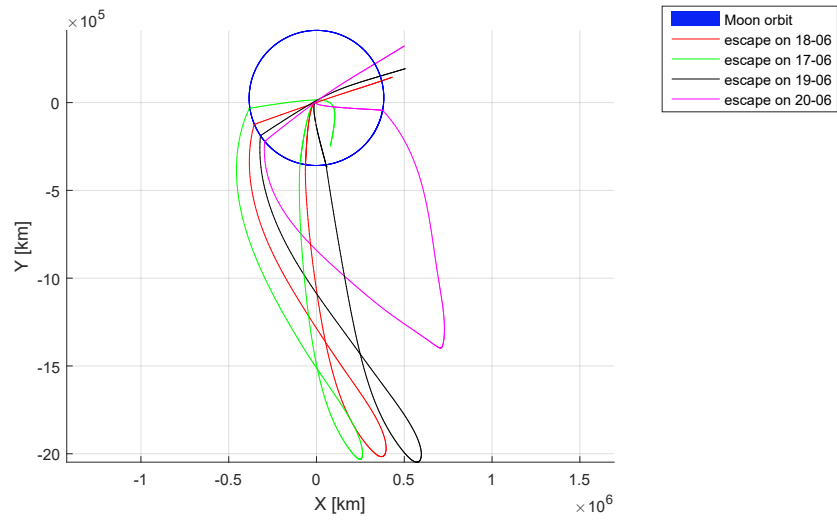


Figure 6.15: a comprehensive, in plane, view of the four different cases

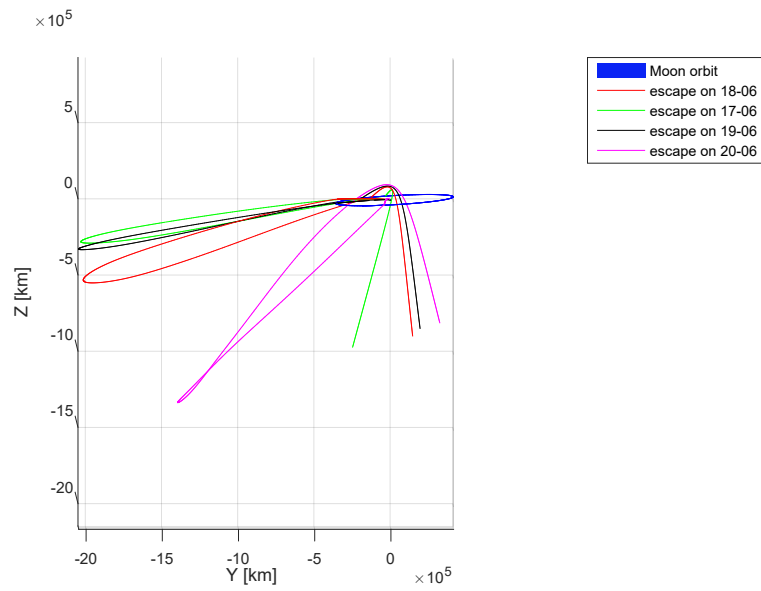


Figure 6.16: a comprehensive, out of plane, view of the four different cases

	case A		case B		case C		case D	
launch	r	1.0302	r	1.0302	r	1.0302	r	1.0302
	θ	1.6440	θ	1.5391	θ	2.0599	θ	3.3867
	ϕ	0.4461	ϕ	0.4452	ϕ	0.4937	ϕ	0.2657
FB1	r	55.566	r	53.951	r	58.081	r	59.842
	θ	4.5201	θ	4.4197	θ	4.8816	θ	6.2038
	ϕ	-0.3810	ϕ	-0.3785	ϕ	-0.4571	ϕ	-0.1164
apogee	r	331.82	r	323.67	r	337.14	r	321.17
	θ	4.9384	θ	4.8537	θ	5.0308	θ	5.4629
	ϕ	-0.6515	ϕ	-0.5370	ϕ	-0.5397	ϕ	-1.0410
FB2	r	59.215	r	60.527	r	58.354	r	58.091
	θ	3.4751	θ	3.2504	θ	3.6533	θ	3.7548
	ϕ	-0.0902	ϕ	0.0235	ϕ	-0.1770	ϕ	-0.2205
escape	r	156.79	r	156.79	r	156.79	r	156.79
	θ	7.1275	θ	7.3874	θ	7.0731	θ	7.1712
	ϕ	-0.8612	ϕ	-1.3959	ϕ	-0.7663	ϕ	-0.6535

Table 6.1: position in spherical coordinates for each phase of the different analyzed cases

	perigee	first flyby	second flyby	escape
case A dates	21-02-2022	23-02-2022	10-06-2022	18-06-2022
case A dimensionless time	—	210	11668	12537
case B dates	20-02-2022	22-02-2022	09-06-2022	17-06-2022
case B dimensionless time	—	203	11637	12513
case C dates	22-02-2022	24-02-2022	10-06-2022	19-06-2022
case C dimensionless time	—	207	11580	12472
case D dates	28-02-2022	02-03-2022	11-06-2022	20-06-2022
case D dimensionless time	—	184	10991	11924

Table 6.2: times of the different analyzed cases

In table 6.2 are reported the times of the most significant points of the escape maneuver. Dimensionless times are used in the shooting method, these quantities are measured starting from a reference point, that is the perigee launch, which is calculated by subtracting the total mission time from the escape time. The escape time is known, while the total mission time (from perigee to escape, t_4 in the p^r vector) has an attempt initial value (at the first iteration) given by the reference solution from the mentioned paper [6].

$$t_4 = 118 \text{ days} * 86400 / t_{conv} = 12636$$

86400 are the seconds in a day, needed to obtain a dimensionless quantity, considering t_{conv} in seconds.

The perigee dimensionless time is not reported in the table, it is the "zero time point".

Finally, the times are transformed in dates for the sake of practicality.

A comparison of the four different solutions is possible in terms of escape mass, that is a final mass with respect to the escape phase, while it is an initial mass with respect to the heliocentric phase.

$$m_{\infty A} = 9822 \text{ kg}$$

$$m_{\infty B} = 9835 \text{ kg}$$

$$m_{\infty C} = 9735 \text{ kg}$$

$$m_{\infty D} = 9522 \text{ kg}$$

Is possible to observe that Case D, which has characterized by a non-planar Moon to Moon leg, is the less efficient solution in terms of escape mass, while case B, the solution that reaches the lower declination on the same phase, has the highest value of the escape mass.

In table 6.3 velocities components and module are reported at the perigee launch and at the escape position. Note that the radial component at the perigee, u_0 , is null among all the analyzed cases, according that was predicted in the analysis description.

	u_0	v_0	w_0	$V_0[km/s]$	u_f	v_f	w_f	$V_f[km/s]$
case A	0.000	1.3553	0.3142	10.998	0.0585	0.0965	-0.1703	1.6145
case B	0.000	1.3542	0.3167	10.994	-0.0113	0.0284	-0.1943	1.5546
case C	0.000	1.3918	0.0888	11.025	0.0734	0.0929	-0.1586	1.5644
case D	0.000	1.2777	0.5792	11.090	0.0679	0.1066	-0.1394	1.4873

Table 6.3: comparison of the velocities at the perigee and at the escape for the analyzed cases

In conclusion, the values of the launch energy escape, C_{3_0} and of the hyperbolic escape energy are reported in table 6.4. Higher value of C_3 correspond to higher value of V_{∞} (which is the same of V_f in table 6.3), according to the definition of the hyperbolic escape energy.

It is important to observe that the case D has the highest value of C_{3_0} (associated with the highest values of V_0), while it has the lower escape energy and velocity. In particular, it has a C_3 lower than C_{3_0} , so the two flybys acting in an undesired way and causing an escape energy loss. This fact remarks, also with regard to the energy, that the last case is the lower efficient solution.

In terms of relative energy variation: Case A are characterized by a significant energy gain, near +350 %, while case B by +280 %, +265 % for case C, and a negative value is shown in the -58 % of case D.

	dimensionless C_{3_0}	C_{3_0}	dimensionless C_3	$C_3 - C_{3_0}$	V_∞
case A	-0.005799	-0.362430 Km^2/s^2	0.014477	0.0203	1.61 Km/s
case B	-0.007215	-0.450906 Km^2/s^2	0.012957	0.0202	1.55 Km/s
case C	0.003611	0.225651 Km^2/s^2	0.013202	0.0096	1.56 Km/s
case D	0.026830	1.676700 Km^2/s^2	0.011320	-0.0155	1.49 Km/s

Table 6.4: energy comparison among the different solutions

Conclusions

In this section a summary of all the fundamental concepts, which are previously analyzed, is given.

In this work a case of a double lunar gravity assist with a solar perturbed lunar-lunar leg is treated. For this maneuver is important to underline the usefulness of each one of the two lunar encounter:

- first flyby is required to reach an apogee characterized by a relative position from Earth and Sun at which the spacecraft path is affected by solar gravity attraction. This perturbation causes the orbit to become a retrograde orbit and, for case A and B (which have a first trailing-side lunar flyby), an energy gain.
- second flyby is necessary to achieve the desired escape conditions, in terms of position and velocity.

All the analyzed cases has an escape that ranging from June 17, 2022 to June 20, 2022, according to an interplanetary mission directed to a Near Earth Asteroid. Launch from perigee occurs on February of the same year. While the first three cases have a duration of near 117 days, Case D is the shorter maneuver with a duration of 112 days.

The advantage of the used gravity assist maneuvers can be highlighted by observing that case A has an energy gain equals to +350 %. This represents the most efficient solution in terms of energy. On the other side, Case D is a solution that achieves the required escape conditions, although it produces a -58% energy loss. In addition, case D is also characterized by the lower value of escape mass, therefore, it can be identified as the less efficient solution.

The second lunar encounter is characterized by a very close passage over the lunar surface. In particular, case B has a periselenium with an altitude of only 39 Km, so special attention is needed if this escape maneuver has to be implemented.

As a result of the imposed constraints and due to convergence necessity of the numerical solution, is not possible to freely vary the escape date and the exact value of the velocity

escape. This fact represents the main drawback of the present study, although remains valid the high efficiency of the escape maneuver which involves a double lunar flybys.

Future development of this work may include a detailed investigation on the different possibilities of escape velocity value, starting from the results obtained in the present document. It is important to remember that the convergence of the system imposes a variation of the current solution by a very little quantities. Also, a check on the radius of the two flybys, in order to avoid an impact with the lunar soil, is needed. However, taking into account the defunding of the ARM mission, a more reasonable future implementation of the presented work should involves the use of a double lunar flyby that enhance the escape energy for realizing a future interplanetary mission by using the procedure illustrated in the present document.

Bibliography

- [1] Howard D. Curtis. *"Orbital mechanics for engineering students"*. Butterworth-Heinemann, 2005.
- [2] Vladimir A. Chobotov *"Orbital mechanics"*. AIAA (American Institute of Aeronautics & Ast), 2002.
- [3] Hanspeter Schaub and John L Junkins. *"Analytical mechanics of space systems"*. Aiaa, 2003.
- [4] Roger R Bate, Donald D Mueller, and Jerry E White. *"Fundamentals of astrodynamics"*. Courier Corporation, 1971.
- [5] Isaac Newton. *"The Principia: mathematical principles of natural philosophy"*. Univ of California Press, 1999.
- [6] Lorenzo Casalino and Gregory Lantoine. *"Design of Lunar-Gravity-Assisted Escape Maneuvres"*. In: 2017 AAS/AIAA Astrodynamics Specialist Conference. AAS/AIAA. Aug. 22, 2017.
- [7] Colasurdo, Guido, and Lorenzo Casalino. *"Indirect methods for the optimization of spacecraft trajectories."*. Modeling and Optimization in Space Engineering. Springer, New York, NY, 2012. 141-158.
- [8] Simeoni, F., Casalino, L., Zavoli, A., and Colasurdo, G.. *"Indirect optimization of satellite deployment into a highly elliptic orbit"*. International Journal of Aerospace Engineering, 2012.
- [9] Maurizio Valesani. *"Escape trajectories exploiting multiple Lunar gravity assists"*. Master thesis. Politecnico di Torino, 2018.
- [10] Sebastiano Bugno. *"Evasion maneuvers with double lunar flyby for interplanetary missions"*. Master thesis. Politecnico di Torino, 2018.
- [11] Ceriotti, Matteo. *"Global optimization of multiple gravity assist trajectories"*. PhD thesis. University of Glasgow, 2010.
- [12] https://en.wikipedia.org/wiki/Space_exploration
- [13] https://en.wikipedia.org/wiki/Voyager_1

- [14] https://it.wikipedia.org/wiki/Programma_Voyager
- [15] <https://history.nasa.gov/conghand/traject.htm>
- [16] https://standards.sedris.org/18026/text/ISOIEC_18026E_RD_ORM.HTM
- [17] <https://www.nasa.gov/content/what-is-nasa-s-asteroid-redirect-mission>
- [18] [https://en.wikipedia.org/wiki/\(341843\)_2008_EV5](https://en.wikipedia.org/wiki/(341843)_2008_EV5)
- [19] <https://solarsystem.nasa.gov/basics/chapter4-1/>